ARTICLE

Arf1-PI4KIIIβ positive vesicles regulate PI(3)P signaling to facilitate lysosomal tubule fission

Maxime Boutry[1], Laura F. DiGiovanni[1,2], Nicholas Demers[1,2], Aaron Fountain[3,4], Sami Mamand[3,4,5], Roberto J. Botelho[3,4], and Peter K. Kim[1,2,6]

Formation and fission of tubules from autolysosomes, endolysosomes, or phagolysosomes are required for lysosome reformation. However, the mechanisms governing these processes in these different lysosomal organelles are poorly understood. Thus, the role of phosphatidylinositol-4-phosphate (PI(4)P) is unclear as it was shown to promote the formation of tubules from phagolysosomes but was proposed to inhibit tubule formation on autolysosomes because the loss of PI4KIIIβ causes extensive lysosomal tubulation. Using super-resolution live-cell imaging, we show that Arf1-PI4KIIIβ positive vesicles are recruited to tubule fission sites from autolysosomes, endolysosomes, and phagolysosomes. Moreover, we show that PI(4)P is required to form autolysosomal tubules and that increased lysosomal tubulation caused by loss of PI4KIIIβ represents impaired tubule fission. At the site of fission, we propose that Arf1-PI4KIIIβ positive vesicles mediate a PI(3)P signal on lysosomes in a process requiring the lipid transfer protein SEC14L2. Our findings indicate that Arf1-PI4KIIIβ positive vesicles and their regulation of PI(3)P are critical components of the lysosomal tubule fission machinery.

Introduction

Lysosomes are degradative organelles and metabolic signaling hubs that play an essential role in cellular homeostasis (Yang and Wang, 2021; Perera and Zoncu, 2016). Dysfunction of lysosomes has been linked to many human diseases ranging from neurodegeneration to metabolic disorders (Parenti et al., 2021; Udayar et al., 2022), highlighting the importance of lysosomal functions for human health. Lysosomes are acidic organelles containing catabolic enzymes enabling the digestion of macromolecules such as proteins, lipids, or carbohydrates. They receive cargos from several pathways, including endocytosis, phagocytosis, and autophagy, in a fusion-dependent manner, generating endolysosomes, phagolysosomes, and autolysosomes, respectively (Yang and Wang, 2021). These parent lysosomal organelles are highly dynamic, undergoing various membrane fission events through vesiculation, splitting, or membrane tubulation (Saffi and Botelho, 2019). In particular, the formation and fission of tubules from the parent lysosomal organelles are needed for recycling lysosomal membrane components to reform competent lysosomes (Yang and Wang, 2021; Yu et al., 2010; Bright et al., 2016; Lancaster et al., 2021). This is vital for regenerating functional lysosomes that were consumed in the formation of the parent lysosomal

organelles. Defects in proteins involved in tubulation and fission are associated with familial forms of neurodegenerative disease, such as Hereditary Spastic Paraplegias and Parkinson's disease, suggesting that lysosomal tubulation is crucial to cellular homeostasis (Chang et al., 2014; Magalhaes et al., 2016). However, the mechanisms for lysosomal tubule formation and fission are still incompletely understood (Saffi and Botelho, 2019).

Lysosome reformation by tubulation can be divided into three general steps (Saffi and Botelho, 2019): the budding step that forms the nascent tubule (Rong et al., 2012); the elongation step; and the fission of the tubule, which involves constriction and scission machinery, including dynamins (Schulze et al., 2013). Although these three steps are shared among the parent lysosomal organelles, it is not clear whether they also share the same molecular machinery or whether specific components exist for each different parent lysosomal organelles (Yang and Wang, 2021).

Phosphoinositides, a group of phospholipids with various degrees of phosphorylation on the inositol headgroup of phosphatidylinositol, act at different steps on the tubulation-mediated recycling of the lysosomal membrane. For instance,

[1]Cell Biology Program, Hospital for Sick Children, Peter Gilgan Centre for Research and Learning, Toronto, Ontario, Canada;   [2]Department of Biochemistry, University of Toronto, Toronto, Ontario, Canada;   [3]Department of Chemistry and Biology, Toronto Metropolitan University, Toronto, Ontario, Canada;   [4]Graduate Program in Molecular Science, Toronto Metropolitan University, Toronto, Ontario, Canada;   [5]Polytechnic Research Center, Erbil Polytechnic University, Erbil, Kurdistan, Iraq;   [6]Department of Biomedical Science and Engineering, Gwangju Institute of Science and Technology, Gwangju, South Korea.

Correspondence to Peter K. Kim: pkim@sickkids.ca.

phosphatidylinositol-4,5-biphosphate (PI(4,5)P$_2$) was shown to mediate tubule extension and the recruitment of the scission machinery for autolysosomes (Saffi and Botelho, 2019; Rong et al., 2012). Additionally, PI(4)P was described to inhibit the formation of tubules from autolysosomes because depletion of PI4KIIIβ (phosphatidylinositol 4-kinase IIIβ)—an enzyme producing PI(4)P—led to extensive tubulation of lysosomes (Sridhar et al., 2013). This proposed a function of PI(4)P differs from recent studies on both the phagolysosomes (Levin-Konigsberg et al., 2019) and endosomes (Jani et al., 2022; Zhu et al., 2022), where PI(4)P was shown to promote the formation of tubules. Thus, whether PI(4)P has a different function in the formation of tubules from autolysosomes compared to phagolysosomes remains unclear.

Recent studies have shown that vesicles carrying markers commonly found in the trans-Golgi network—including Arf1 (ADP-ribosylation factor 1), PI4KIIIβ, and TGN46—contribute to both the mitochondrial division process (Nagashima et al., 2020) and the fission of Rab5-positive early endosomes (Gong et al., 2021). Both studies showed Arf1 positive vesicles at the site of fission, and that inactivation of Arf1 or inhibition of PI4KIIIβ, which are expected to disrupt the formation of Golgi-derived vesicles, resulted in impaired mitochondria and endosome fission. Together, these studies indicate that Arf1 and PI4KIIIβ activities are required for the formation and/or function of these vesicles at the sites of fission. Based on these studies, we hypothesized that vesicles positive for Arf1 and PI4KIIIβ also play a role in the fission of lysosomal tubules from parent lysosomal organelles. Specifically, the extensive tubulation of lysosomes observed in PI4KIIIβ-depleted cells (Sridhar et al., 2013) may be due to defective fission resulting from a loss of formation and/or function of these vesicles at lysosomal tubule fission sites.

Using live-cell super-resolution microscopy, we show here that Arf1-PI4KIIIβ positive vesicles are recruited to the fission site of lysosomal tubules from several parent lysosome organelles. Our results support that they contribute to this process by mediating phosphatidylinositol-3-phosphate (PI(3)P) signaling on the lysosome at the site of fission.

Results

Arf1 positive vesicles and Lamp1 positive organelles form dynamic contacts

To test our hypothesis that vesicles positive for Arf1 and PI4KIIIβ contribute to the fission of lysosomal tubules, we first examined for interactions between Arf1 positive vesicles and lysosomes. We used GFP-tagged Arf1 (Arf1-GFP), which localizes to both the trans-Golgi network and vesicles and that was previously used as a marker for Arf1 positive vesicles in membrane fission events (Nagashima et al., 2020; Gong et al., 2021; Boutry and Kim, 2021), and the mCherry tagged late endosomal/lysosomal marker Lamp1 (Eskelinen et al., 2003; Eskelinen, 2006). Lattice light-sheet microscopy (LLSM) time-lapse imaging performed on mouse embryonic fibroblasts (MEFs) showed Lamp1 positive organelles and Arf1-GFP positive vesicles juxtaposed to each other for a prolonged time (Fig. 1 A). To determine whether these two compartments are forming membrane contact, we imaged

them in live cells using a sub-Airy pinhole confocal super-resolution microscopy. We found that Arf1 positive vesicle and Lamp1 positive organelle interactions were stable and dynamic in MEFs (Fig. 1, B and C; and Video 1) and HeLa cells (Fig. S1 A). About 20% of Lamp1 positive organelles in both cell types appeared in contact with at least one Arf1 positive vesicle at any given time (Fig. 1 D and Fig. S1 B) and had a mean minimum duration of contact of ~45 s (Fig. 1 E and Fig. S1 C). Interestingly, we also observed Arf1 positive vesicles localized in juxtaposition to the site of Lamp1 positive organelle tubule fission (Fig. 1 F and Video 2). To explore the significance of Arf1-positive vesicles at the site of Lamp1 positive vesicle fission, we promoted the formation and fission of tubules from Lamp1 organelles by starving cells for 8 h in amino acid-free media (Hanks' Balanced Salt Solution [HBSS]) as previously described (Yu et al., 2010; Rong et al., 2012). In live cell images, we observed that Arf1-GFP positive vesicles marked more than half of the sites of tubule fission from Lamp1 positive organelles in MEFs (Fig. 1 G) and HeLa cells (Fig. S1 D). To ensure that the presence of Arf1 positive vesicles at Lamp1 positive tubule fission sites was not due to random positioning of the two structures, we re-quantified the same data where the Lamp1-mCherry signal was rotated by 90°. The resulting quantification was significantly lower than the original images (Fig. 1 G). Since overexpressed Lamp1 is not restricted to late endosomes/lysosomes but can also mark early endosomes (Saric et al., 2021), we examined the cells for lysosome tubule fission from Lamp1 positive organelles that were acidic (cresyl violet [Ostrowski et al., 2016] positive), or that contained overnight chased fluorescent 10 kD Dextran (Johnson et al., 2016). This revealed that Arf1-GFP positive vesicles mark lysosomal tubule fission sites (Fig. 1 H and Fig. S1 E). Taken together, our data suggest that Arf1 positive vesicles and Lamp1 organelles interact with each other and that these contacts are formed at or near the site of lysosomal tubule fission.

Arf1 vesicles at lysosomal tubule fission sites are positive for trans-Golgi network markers but not endosomal markers

Since vesicles implicated in mitochondrial fission were reported to be positive for both PI4KIIIβ and TGN46 (Nagashima et al., 2020), we exogenously expressed fluorescent protein tagged versions of these proteins in MEFs and treated them with amino acid-free media (HBSS) for 8 h to promote fission of tubules from Lamp1 positive organelles. We found that GFP-PI4KIIIβ positive vesicles and TGN46-mEmerald positive vesicles were recruited to approximately half of the observed Lamp1 positive organelle tubule fission events (Fig. 2, A and B), similar to that of Arf1 positive vesicles (Fig. 1 G). Importantly, we observed that vesicles recruited to tubule fission sites were positive for both Arf1 and PI4KIIIβ (Fig. 2 C). This supports the notion that vesicles marking the sites of Lamp1 tubule fission are positive for Arf1, PI4KIIIβ, and TGN46. Hereafter, we refer to these vesicles as Arf1-PI4KIIIβ positive vesicles.

As Arf1 and TGN46 were described to localize to non-Golgi-derived vesicles such as endosomes (Nakai et al., 2013; Saint-Pol et al., 2004), we repeated Lamp1 tubule fission experiments in cells co-transfected with the GFP tagged early endosome markers Rab5 or EEA1, or with the recycling endosome marker CFP-

Figure 1. **Arf1 positive vesicles make stable and dynamic contacts with Lamp1 positive organelles and mark lysosomal tubule fission sites. (A)** LLSM imaging of a MEF expressing Lamp1-mCherry and Arf1-GFP. Insets show that Arf1 positive vesicles and Lamp1 positive organelles appear to make stable contact over time. Scale bars: 10 and 1 μm (inset). **(B)** Representative super-resolution image of a MEF cell expressing Arf1-GFP and Lamp1-mCherry. Inset shows a contact between an Arf1 positive vesicle and a Lamp1 positive organelle. Side panels show the view along the z-axis. Scale bar: 10 and 1 μm (inset). **(C)** Representative time-lapse images of two Lamp1 positive organelle-Arf1 positive vesicle contacts. Yellow arrows indicate contacts, and the red arrow indicates contact untethering. Scale bars: 1 μm. **(D)** Quantification of the percentage of Lamp1 positive organelles in contact with at least one Arf1 positive vesicle in MEFs. The mean ± SEM from three independent experiments is shown. **(E)** Quantification of the mean minimum duration of

Lamp1 positive organelle-Arf1 positive vesicle contacts in seconds. 400 randomly chosen contacts from 40 MEFs were analyzed. **(F)** LLSM imaging of a MEF cell expressing Lamp1-mCherry and Arf1-GFP. Insets show time-lapse images of a single plane of only Lamp1-mCherry (inverted images) along with the corresponding merge and 3D reconstruction of a Lamp1 positive tubule fission event showing recruitment of an Arf1 positive vesicle at the fission site. Scale bars: 10 and 1 µm (insets). **(G)** Representative time-lapse imaging showing an Arf1-GFP positive vesicle marking the fission site of tubule from a Lamp1-mCherry positive organelle in a MEF cell starved for 8 h with HBSS (amino acid-free media). Yellow arrows indicate the fission event. The bottom panels are the same images, but the Lamp1-mCherry channel was rotated by 90°. Scale bar: 2 µm. The percentage of tubule fission events marked by Arf1-GFP vesicles was quantified along with the same data but where the Lamp1-mCherry channel was rotated by 90°. P value from a Fisher's exact test, two-sided unpaired t test is shown. **(H)** Representative time-lapse imaging showing an Arf1-GFP vesicle marking the fission site of a tubule from a lysosome (Lamp1-SNAP/cresyl violet positive). Yellow arrow indicates fission. Scale bar: 1 µm.

Rab11 (Elkin et al., 2016). The percentage of Lamp1 tubule fission events marked by vesicles positive for these markers was much lower than those observed for Arf1, PI4KIIIβ, and TGN46 (Fig. 2, D–G). Instead, their localization to the site of fission was similar to our negative control images, where Lamp1 images were rotated by 90° (Fig. 2 G). Moreover, there was no significant colocalization of these markers with Arf1 positive vesicles in resting cells (Fig. 2, H and I), whereas we observed an extensive colocalization with PI4KIIIβ, consistent with the literature (Waugh, 2019). The higher colocalization between Arf1 and Rab11 compared to Rab5 suggests that some Arf1 puncta are recycling endosomes. Interestingly, Rab11 was described to localize to post-Golgi vesicles (Welz et al., 2014), which could also explain the moderate colocalization observed here. However, the low percentage of tubule fission events marked by Rab11 compared to that of Arf1 positive vesicles indicates that the Arf1 positive vesicles recruited to fission sites are not recycling endosomes.

Taken together, our results indicate that Arf1-PI4KIIIβ positive vesicles that are recruited to Lamp1 positive organelle tubule fission sites are unlikely to be endosomal vesicles. Instead, our findings strongly suggest that they more closely resemble vesicles derived from the Golgi apparatus.

Arf1-PI4KIIIβ positive vesicles mark multiple types of lysosomal tubule fission events

Lysosome reformation from autolysosomes, endolysosomes, and phagolysosomes involves membrane tubulation and fission (Fig. 3 A; Yang and Wang, 2021). To address whether Arf1-PI4KIIIβ positive vesicles contribute to the fission of tubules from all these lysosomal organelles, we first examined their recruitment at autolysosomal tubule fission sites. The formation of tubules from autolysosomes was triggered by incubating cells in amino acid-free media (HBSS) for 8 h, at which time the formation of tubules from autolysosomes was shown to peak in multiple cell lines (Yu et al., 2010). We identified autolysosomes as organelles positive for the membrane marker Lamp1 and the autophagic marker mCherry-LC3. We observed that Arf1 positive vesicles were present at more than half of the tubule fission events from autolysosomes in COS7 cells (Fig. 3 B and Video 3), suggesting that Arf1-PI4KIIIβ positive vesicles contribute to the fission of autolysosomal tubules.

As the ER was previously shown to play an important role in the fission of Rab7 positive endosomes (Hoyer et al., 2018), we visualized whether it was present at the site of tubule fission marked by Arf1 positive vesicles. The ER marked almost all tubule division sites (Fig. S2 A), suggesting that the recruitment

and/or the function of Arf1-PI4KIIIβ positive vesicles at the fission site involves the formation of a three-way contact between the vesicles, the ER, and lysosomes. As many organelles form extensive contacts with the ER (Wu et al., 2018), the localization of the Arf1-PI4KIIIβ positive vesicles at the sites of Lamp1 tubule fission may be a result of their co-incidence on the ER, instead of active recruitment to the site of division. To test this possibility, we monitored for the presence of peroxisomes at Lamp1 tubules fission sites as these small punctate structures appear virtually always in contact with the ER (Hua et al., 2017; Costello et al., 2017). We found that the percentage of Lamp1 tubule fission events marked by peroxisomes (ub-RFP-SKL [Aranovich et al., 2014]) was not significantly different from that expected by chance (Fig. S2 B). Thus, giving further support for Arf1-PI4KIIIβ positive vesicles being specifically localized to sites of tubule fission of Lamp1 positive organelles.

To examine whether Arf1-PI4KIIIβ positive vesicles also localized to fission events of tubules extruding from endolysosomes, we promoted the formation of endolysosomes by incubating cells for 24 h in media containing 30 mM of sucrose. Sucrose is endocytosed and reaches lysosomes via the fusion of endosomes with lysosomes, forming endolysosomes called sucrosomes (Bright et al., 2016). As lysosomes in mammalian cells are unable to digest sucrose, this disaccharide accumulates in endolysosomes, inducing their swelling. The endolysosome swelling was relieved by incubating the cells with 0.5 mg/ml of invertase, a yeast enzyme that hydrolyses sucrose, which reaches the swollen endolysosomes via the endocytic pathway, allowing a return to normal lysosome size (Fig. 3 C) in a reformation process implicating the formation and fission of tubules (Bright et al., 2016). Arf1 positive vesicles were observed at more than half of tubule fission events from sucrose-induced endolysosomes (Fig. 3 D) that were identified as positive for Lamp1 and overnight chased fluorescent 10 kD Dextran (endocytosed cargo). Similarly, GFP-PI4KIIIβ positive vesicles were also found at endolysosomal tubule fission sites (Fig. S2 C), supporting that Arf1-PI4KIIIβ positive vesicles mark sites of tubule fission from endolysosomes.

For the recycling of phagolysosomal membrane, we used RAW 264.7 macrophages incubated with opsonized sheep red blood cells (SRBCs; Levin et al., 2017). We imaged RAW 264.7 cells 15 min after incubation with SRBCs to allow for the formation of phagolysosomes that were Lamp1 positive. Similar to the other lysosomal organelles, both Arf1-GFP and GFP-PI4KIIIβ were observed as being recruited to tubule fission events (Fig. 3, E and F; and Video 4 and Fig. S2 D). These results support that

Figure 2. **Arf1 positive vesicles recruited to Lamp1 positive organelles tubule fission sites are positive for PI4KIIIβ and TGN46 but negative for endosome markers. (A and B)** Time-lapse images and quantification of MEFs incubated for 8 h in HBSS media showing GFP-PI4KIIIβ (A) or TGN46-mEmerald (B) positive vesicles at the sites of Lamp1 positive tubule fission. Yellow arrows indicate fission. Scale bars: 2 μm. **(C)** Representative time-lapse images of a MEF as in A but showing a Lamp1-mCherry tubule fission event marked by a vesicle positive for both Arf1-SNAP and GFP-PI4KIIIβ. Yellow arrow indicates fission. Scale bar: 1 μm. **(D–F)** Time-lapse images of MEFs expressing Lamp1-mCherry and (D) GFP-Rab5, (E) GFP-EEA1, or (F) CFP-Rab11 incubated for 8 h in HBSS media. Yellow arrows indicate fission. Scale bars: 1 μm. **(G)** Quantification of vesicles positive for proteins in D–F shows them to be absent at Lamp1

positive tubule fission events. Also shown is the quantification of images in D where lamp1 was rotated by 90°. **(H)** Representative images of MEFs expressing Arf1-SNAP with GFP-Rab5, GFP-EEA1, CFP-Rab11, or GFP-PI4KIIIβ. Scale bar: 5 μm. **(I)** Pearson's coefficient measurement of cells is described in H as indicated. The graph shows the mean ± SEM from three independent experiments. One-way ANOVA with Dunnett's multiple comparison test. The number of events and cells quantified are shown with each quantification data.

Arf1-PI4KIIIβ positive vesicles are recruited to the fission sites of phagolysosomal tubules.

Finally, we tested whether Arf1-PI4KIIIβ positive vesicles are also recruited to fission sites of lysosomal reformation tubules without specifically promoting the formation of endolysosomes, autolysosomes, or phagolysosomes. We abolished the balance between fusion and fission of lysosomes by the short-term reversible inhibition of PIKfyve, the enzyme responsible for producing $PI(3,5)P_2$ on lysosomes, using the PIKfyve inhibitor YM201636 (Saffi and Botelho, 2019; Choy et al., 2018). Inhibition of PIKfyve leads to larger and fewer lysosomes (Saffi and Botelho, 2019; Choy et al., 2018; Bissig et al., 2017). Washout of the inhibitor restored the balance between fusion and fission, leading to a recovery of lysosome size (Fig. 3 G) that involves the formation and fission of tubules. We found again that about 60% of fission events showed recruitment of an Arf1 positive vesicle (Fig. 3, H and I). These Lamp1 positive structures generated by short-term PIKfyve inhibition were negative for Rab5, indicating they are not endosome-like organelles (Fig. S3 A). Nor were they autolysosomes as short-term PIKfyve inhibition did not induce autophagy (Fig. S3 B), and the Lamp1 structures were not positive for the autophagic marker LC3 (Fig. S3 C). Taken together, our data show that Arf1-PI4KIIIβ positive vesicles are recruited to various types of lysosomal tubule fission events, suggesting that they contribute to the fission of lysosomal tubules.

Arf1 inactivation and PI4KIIIβ inhibition impair the fission of lysosomal tubules

To test whether Arf1-PI4KIIIβ positive vesicles are required for the fission of lysosomal tubules, we examined whether inhibiting Arf1 activation or PI4KIIIβ function increased the number of lysosomal tubules. Such a phenotype is expected when the fission of tubules is impaired (Chang et al., 2014; Schulze et al., 2013), as demonstrated by the chemical inhibition of dynamins that contribute to tubule scission from lysosomes (Fig. 4, A and B). The chemical inhibition of PI4KIIIβ was performed with PI4KIIIbeta-IN-10 (Crivelli et al., 2022), and Arf1 was inactivated by treating cells with Brefeldin A (BFA; Niu et al., 2005). PI4KIIIbeta-IN-10 treatment significantly reduced the number of Arf1 positive vesicles and PI4KIIIβ positive vesicles, while BFA led to a near complete loss of vesicular signal from both Arf1-GFP and GFP-PI4KIIIβ, suggesting that these treatments inhibited the formation of Arf1–PI4KIIIβ positive vesicles (Fig. S4, A–D). Treatments with PI4KIIIbeta-IN-10 or BFA strongly increased the numbers of lysosomal tubules compared to vehicle control-treated cells (Fig. 4, C and D). Consistently, an increased number of tubules from Lamp1 positive organelles was also observed in BFA-treated HEK293 cells (Fig. S4, E and F) and in primary mouse macrophages where lysosomes were marked using chased fluorescent 10 kD Dextran (Fig. S4, G and H). Lipopolysaccharide (LPS) treatment, which induces striking lysosomal

tubulation in primary macrophages (Saric et al., 2016), was used as a positive control.

To determine whether the elevated number of lysosomal tubules was due to a decrease in fission, we quantified the rate of tubule fission. Both PI4KIIIbeta-IN-10 and BFA treatment significantly reduced the rate of fission (number of fission events normalized by time and cell volume) of tubules from Lamp1 positive organelles compared to vehicle-treated MEFs (Fig. 4, E and F) when autolysosomal tubules were induced by prolonged starvation (HBSS, 8 h). Similar results were observed for endolysosomes and phagolysosomes. BFA treatment caused an increase in the number of Lamp1 tubules in sucrosomes (endolysosomes) to levels similar to cells where scission was inhibited by Dynasore treatment (Fig. 4, G and H). In RAW 264.7 cells undergoing phagocytosis of SRBCs, BFA treatment for 30 min after the formation of phagolysosomes (15 min after phagocytosis synchronization) resulted in an increase in the number of tubules per phagolysosomes (Fig. 4 I) compared to vehicle-treated cells. We validated the change in tubules in phagolysosomes using the PI(4)P biosensor 2xP4M that was previously shown to allow visualization of tubules emerging from phagolysosomes (Levin-Konigsberg et al., 2019; Fig. S4 I). Finally, we examined whether Arf1 was required for tubule fission in lysosomes recovering from PIKfyve inhibition. After YM201636 washout, a decrease in tubule fission rate was observed in Lamp1 positive organelles in cells treated with BFA during the washout compared to control cells (Fig. 4 J) that was accordingly linked to an increase in Lamp1 tubules (Fig. S4, J and K). Together, our data show that inhibiting the formation and/or function of Arf1-PI4KIIIβ positive vesicles impairs the fission of tubules from lysosomes. Thus, giving support for a mechanism where Arf1-PI4KIIIβ positive vesicles actively contribute to the lysosomal tubule fission process.

Arf1-PI4KIIIβ positive vesicles are not required for lysosome vesiculation or splitting

Lysosomal membrane fission occurs not only via tubulation but also by vesiculation and splitting (Saffi and Botelho, 2019). Tubulation allows for the enrichment of membrane components and the exclusion of lumen/cargo content, while vesiculation and splitting allow for the trafficking of luminal components and cargos (Saffi and Botelho, 2019). To test whether Arf1-PI4KIIIβ positive vesicles are also involved in fission by vesiculation and splitting, we inhibited their function and/or formation using PIK93 (PI4KIIIβ inhibitor) or BFA. We then followed the fragmentation of phagolysosomes containing mRFP-labeled *Escherichia coli* in RAW 264.7 cells. After engulfment of the prey into a phagosome and fusion with lysosomes, phagolysosomes undergo extensive fragmentation that involves tubulation, vesiculation, and splitting (Lancaster et al., 2021). By monitoring the phagolysosome cargo (i.e., mRFP-*E. coli*) and not the membrane protein, we can specifically evaluate vesiculation and splitting forms of
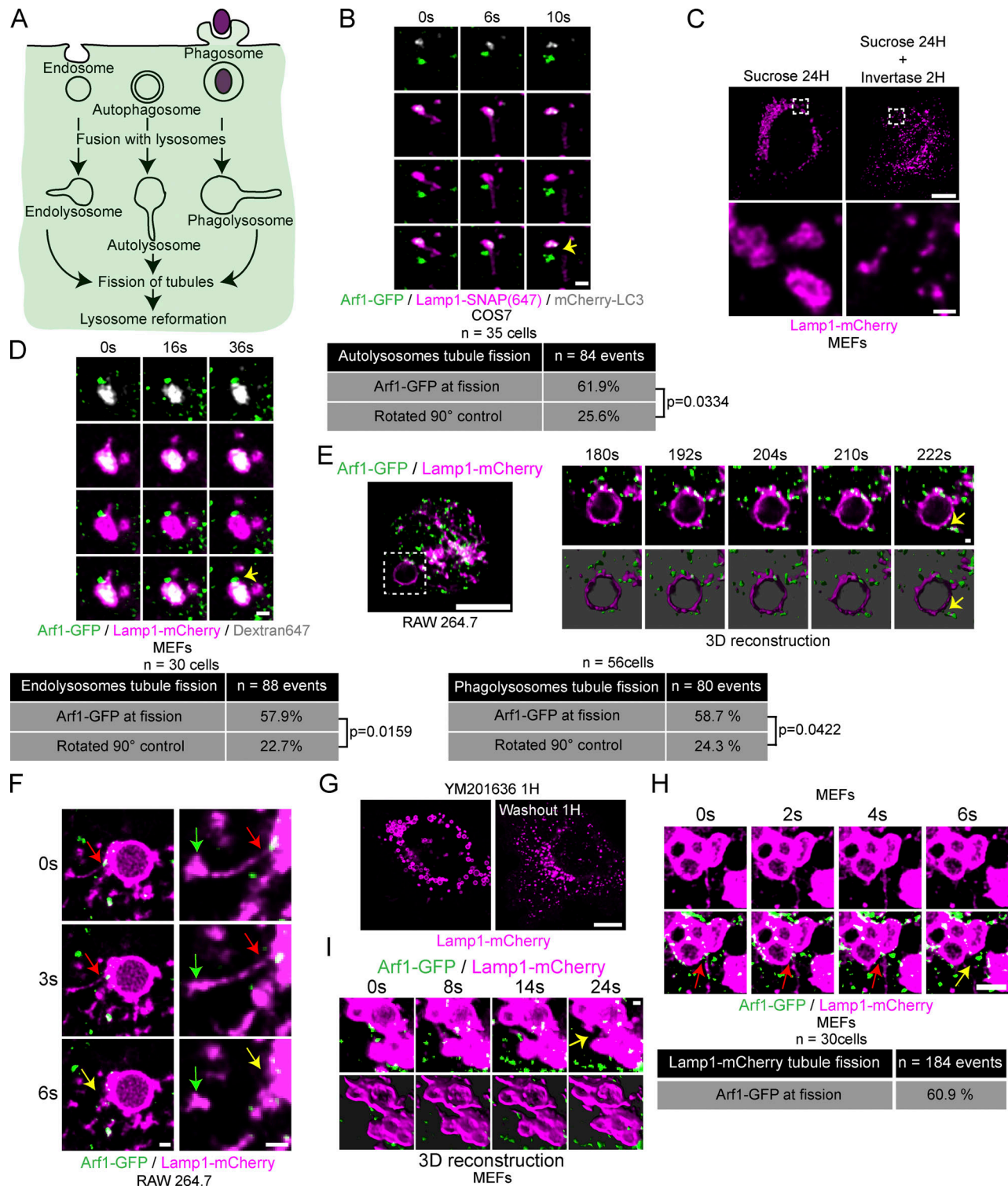
Figure 3. **Arf1 positive vesicles mark fission sites of tubules extending from autolysosomes, endolysosomes, phagolysosomes, and lysosomes.** **(A)** Cartoon illustration of endocytosis, autophagy, phagocytosis, and lysosome reformation occurring in these processes. **(B)** Time-lapse images of a COS7 cell showing an autolysosomal (Lamp1+/LC3+) tubule fission event marked by an Arf1 positive vesicle and quantification of such events, *n* = 84 events from 35 COS7 cells. P value from a Fisher's exact test, two-sided unpaired *t* test is shown. Yellow arrow indicates fission. Scale bar: 1 μm. **(C)** MEFs were incubated with 30 mM sucrose for 24 h to induce the formation of swollen endolysosomes (sucrosomes). The swelling was relieved using Invertase (0.5 mg/ml 2 h) to digest sucrose to restore lysosomes. Scale bars: 10 and 1 μm (insets). **(D)** Time-lapse images of MEFs showing an endolysosomal (Lamp1+/Dextran+) tubule fission event marked by an Arf1 positive vesicle and quantification of such events, *n* = 88 events from 30 MEFs. P value from a Fisher's exact test, two-sided unpaired *t* test is shown. Lamp1-mCherry signal rotated by 90° was used as a negative control. Yellow arrow indicates fission. Scale bar: 1 μm. **(E and F)** RAW264.7 macrophages were fed opsonized SRBCs, and phagocytosis was synchronized via centrifugation. Live-cell timelapse images showing Arf1-GFP vesicles at phagolysosomal tubule fission sites using LLSM and its 3D reconstruction (bottom panels; E) and live

confocal microscopy (F). Red and yellow arrows indicate tubule neck and tubule fission, respectively. The green arrows indicate the tip of the tubule. Scale bars: 10 μm for E; 1 μm for inset in E and F. Quantification of such events, *n* = 80 events from 56 RAW 264.7 cells. P value from a Fisher's exact test, two-sided unpaired *t* test is shown. Lamp1-mCherry signal rotated by 90° was used as a negative control. **(G)** MEFs were treated with reversible PIKfyve inhibitor YM201636 (1 μM for 1 h) to promote swelling of lysosomes. Washout of the inhibitor allows a return to normal lysosomal size via lysosome reformation in about an hour. Scale bar: 10 μm. **(H and I)** Time-lapse confocal images of a Lamp1 positive tubule fission event post-YM201636 washout showing recruitment of an Arf1 positive vesicle with quantification of such events (H) *n* = 184 events from 30 MEFs and LLSM images with three-dimensional reconstruction (I). Images were acquired 5–40 min after inhibitor washout. Red and yellow arrows indicate tubule neck and tubule fission, respectively. Scale bars: 2 μm (H) and 1 μm (I).

divisions. Interestingly, inhibition of PI4KIIIβ or Arf1 inactivation had no significant effect on phagolysosome fragmentation compared to vehicle-treated control (Fig. S5, A and B). Ikarugamycin, which inhibits clathrin, was used as a positive control. This indicates that Arf1-PI4KIIIβ positive vesicles are dispensable for phagolysosome fragmentation by lysosomal vesiculation and splitting. To confirm this result, we followed the fission of the Lamp1 positive organelle after PIKfyve inhibition and washout. Analysis of 345 Lamp1 positive organelles from 23 cells (15 randomly chosen Lamp1 positive organelles analyzed per cell) treated with BFA or a vehicle control showed impaired fission of tubules but not of vesicles (vesiculation; Fig. S5 C).

PI4KIIIβ inhibition increases the number of lysosomal tubules by impairing their fission

Our results suggest that inhibiting PI4KIIIβ, a factor required for the formation and/or function of Arf1-PI4KIIIβ positive vesicles, increases the number of lysosomal tubules due to impaired tubule fission (Fig. 4, C–E). It was previously proposed that PI4KIIIβ downregulation caused extensive lysosomal tubulation due to a loss of PI(4)P production by PI4KIIIβ at lysosomes, and thus PI(4)P produced by PI4KIIIβ at lysosomes inhibits the formation of tubules (Sridhar et al., 2013). However, we find that PI(4)P was readily detected on tubules emerging from Lamp1 positive organelles after prolonged starvation and phagolysosomes (Fig. 5, A and B; and Fig. S4 I), suggesting that lysosomal tubulation caused by loss of PI4KIIIβ function could be unrelated to its potential role in PI(4)P production at lysosomes. This hypothesis is further supported by the recent report that PI4KIIIβ does not play a major role in PI(4)P synthesis at lysosomes (Baba et al., 2019). To test whether the production of PI(4)P by PI4KIIIβ at lysosomes inhibits the formation of tubules from lysosomes, we anchored PI4KIIIβ to lysosomes by fusing it to the LysoGFP tag composed of the lysosomal anchoring sequence of p18 (Lim et al., 2019) fused to GFP (Fig. 5 C). Overexpression of LysoGFP-PI4KIIIβ in MEFs led to increased levels of the PI(4)P biosensor mCherry-P4M (Hammond et al., 2014) at Lamp1 positive organelles compared to the control Lamp1-GFP vector (Fig. S6, A and B) supporting that it produced PI(4)P at lysosomes. However, lysoGFP-PI4KIIIβ was detected on Lamp1-mCherry positive tubules when the formation of tubules from autolysosomes was promoted by prolonged starvation, and its mediation of an increase in lysosomal PI(4)P had no effect on the number of Lamp1-mCherry tubules compared to Lamp1-GFP expressing control cells at a basal state or after prolonged starvation (Fig. 5, D and E). These results strongly suggest that the localization of PI4KIIIβ and its production of PI(4)P at lysosomes do not inhibit the formation of autolysosomal tubules.

To further clarify the role of lysosomal PI(4)P in the regulation of lysosomal tubules, we targeted the PI(4)P phosphatase Sac1 to late endosomes/lysosomes and monitored the number of Lamp1 tubules after prolonged starvation. First, we overexpressed GFP-ORPSAC1, where the catalytic domain of Sac1 replaces the lipid transfer domain of ORP1L, a late endosomal/lysosomal localized protein. This construct was previously successfully used to deplete PI(4)P levels at lysosomes (Levin-Konigsberg et al., 2019; Boutry and Kim, 2021). Overexpression of ORPSAC1 in MEFs led to fewer Lamp1 tubules after starvation compared to overexpression of the catalytic dead mutant C392S (Fig. S6, C and D). Similar but stronger inhibition was observed in both resting and starved MEFs when lysosomal PI(4)P was depleted using the LysoGFP-Sac1 construct (Fig. 5, F–H), causing a decreased P4M signal at Lamp1 positive organelles compared to the catalytically dead mutant LysoGFP-Sac1 C389S (Fig. S6, E and F). This result was also confirmed in HeLa cells (Fig. S6, G and H). Finally, as PI(4)P was proposed to promote the fusion of autophagosomes with lysosomes to form autolysosomes (Wang et al., 2015), we examined whether the expression of LysoGFP-Sac1 impaired autolysosome formation. LysoGFP-Sac1 overexpression had no effect on the colocalization of Lamp1 with the autophagosome marker mCherry-LC3 during starvation (Fig. S6, I and J) or on the loss of peroxisomes by pexophagy (Fig. S6, K and L), a substrate of starvation-induced autophagy (Germain and Kim, 2020). These results indicate that depletion of PI(4)P by LysoGFP-Sac1 did not impair the fusion of lysosomes with autophagosomes. Thus, our data support that lysosomal PI(4)P is required to generate tubules on lysosomes and that PI4KIIIβ has no anti-tubulation role at lysosomes. Instead, our data suggest that PI4KIIIβ plays a role in lysosomal tubule fission by mediating the formation and/or function of Arf1-PI4KIIIβ positive vesicles that contribute to the fission of lysosomal tubules.

Arf1-PI4KIIIβ positive vesicles at Lamp1 tubule fission sites are associated with a PI(3)P signal

Next, we investigated the role of Arf1-PI4KIIIβ positive vesicles in the lysosomal tubule fission process. Recently, a subset of Arf1 positive vesicles was shown to contribute to the fission of Rab5 positive early endosomes by promoting a phosphatidylinositol-3-phosphate (PI(3)P) increase on the dividing endosome (Gong et al., 2021). Therefore, we investigated whether Arf1-PI4KIIIβ positive vesicles could perform a similar role for the fission of lysosomal tubules. We first examined whether Lamp1 tubule fission events were associated with a modulation of PI(3)P. We starved MEFs with amino acid-free media (HBSS) for 8 h to promote the formation and fission of Lamp1 tubules and
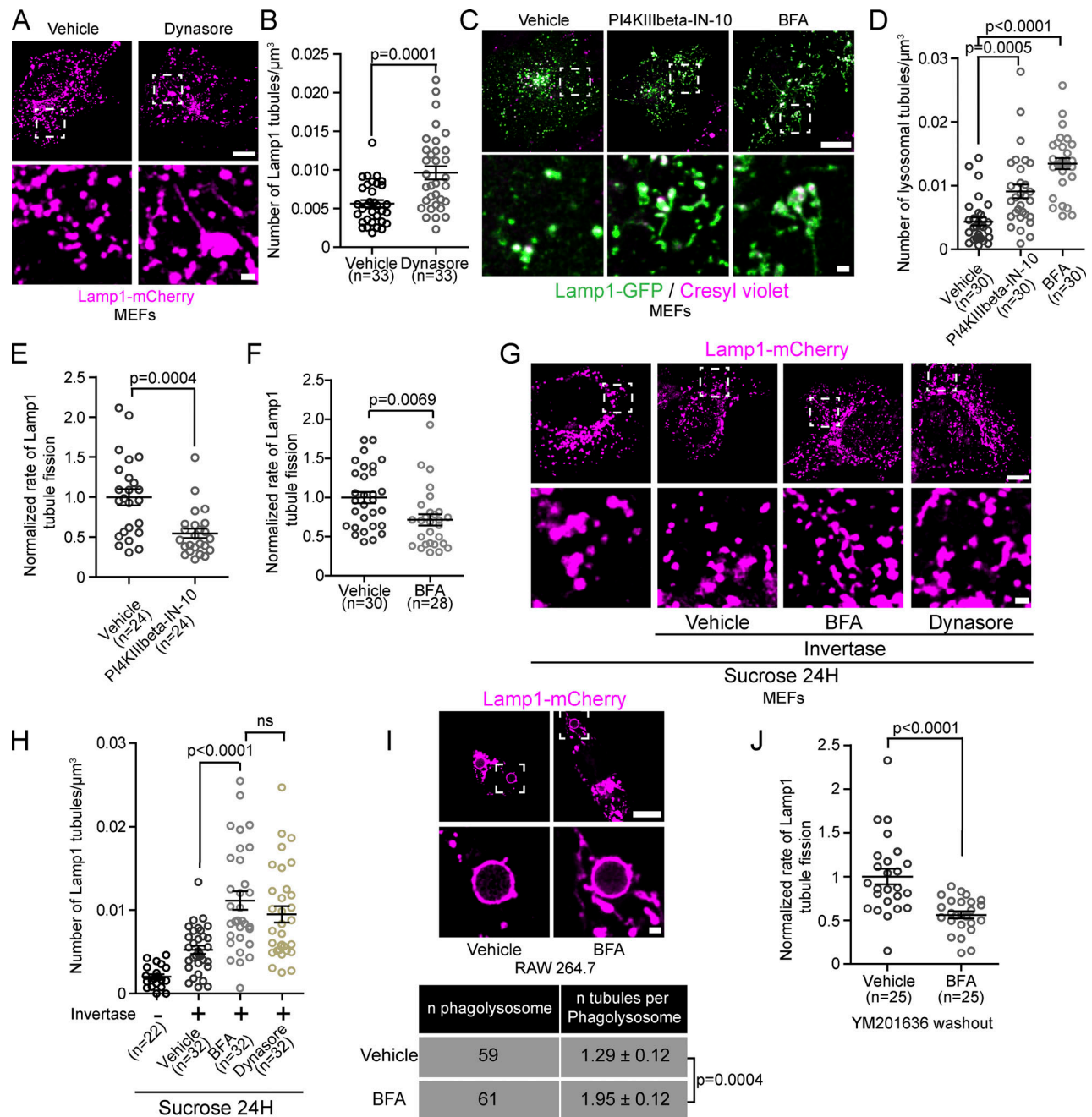
Figure 4. **Inhibition of Arf1 activation or PI4KIIIβ function impairs the fission of lysosomal tubules. (A and B)** MEFs expressing Lamp1-mCherry and treated with Dynasore (40 μM) for 2 h show increased Lamp1 positive tubule numbers (A). Scale bars: 10 and 1 μm (inset). Quantification of the number of lysosomal tubules (B). Two-sided unpaired *t* test. **(C)** MEFs treated with the PI4KIIIβ inhibitor PI4KIIIbeta-IN-10 (25 nM for 3 h) or Arf1 activation inhibitor Brefeldin A (BFA; 10 μg/ml) and stained with the acidic marker cresyl violet. Scale bars: 10 and 1 μm (inset). **(D)** Quantification of the number of lysosomal tubules in cells described in C. One-way ANOVA with Dunnett's multiple comparison test. **(E and F)** Normalized rate of Lamp1 positive tubule fission in MEFs starved for 8 h in HBSS and treated with PI4KIIIbeta-IN-10 (3 h; E) or with BFA (1 h) before imaging (F). Two-sided, unpaired *t* test. **(G)** Representative images of endolysosomes (sucrosomes) tubule formation assay in MEFs. After 1 h invertase treatment, cells were treated with BFA or Dynasore for 1 h and imaged. An equal volume of ethanol was used as vehicle control. Scale bar: 10 μm. **(H)** Quantification of the number of Lamp1 positive tubules of conditions in G. One-way ANOVA with Dunnett's multiple comparison test. **(I)** Representative images of phagolysosomes in RAW 264.7 cells phagocyting SRBCs (scale bar: 10 μm) and quantification of the number of tubules per phagosome in cells treated with BFA (30 min) or vehicle control (Ethanol, 30 min). Two-sided unpaired *t* test. **(J)** Normalized rate of Lamp1 positive tubule fission in MEFs after inhibition of PIKfyve (YM201636 1 μM, 1 h) and washout of the drug in the presence of BFA or vehicle control. Two-sided unpaired *t* test. **(B, D–H, and J)**. *n* = number of cells per condition. All graphs show the mean ± SEM from three independent experiments.
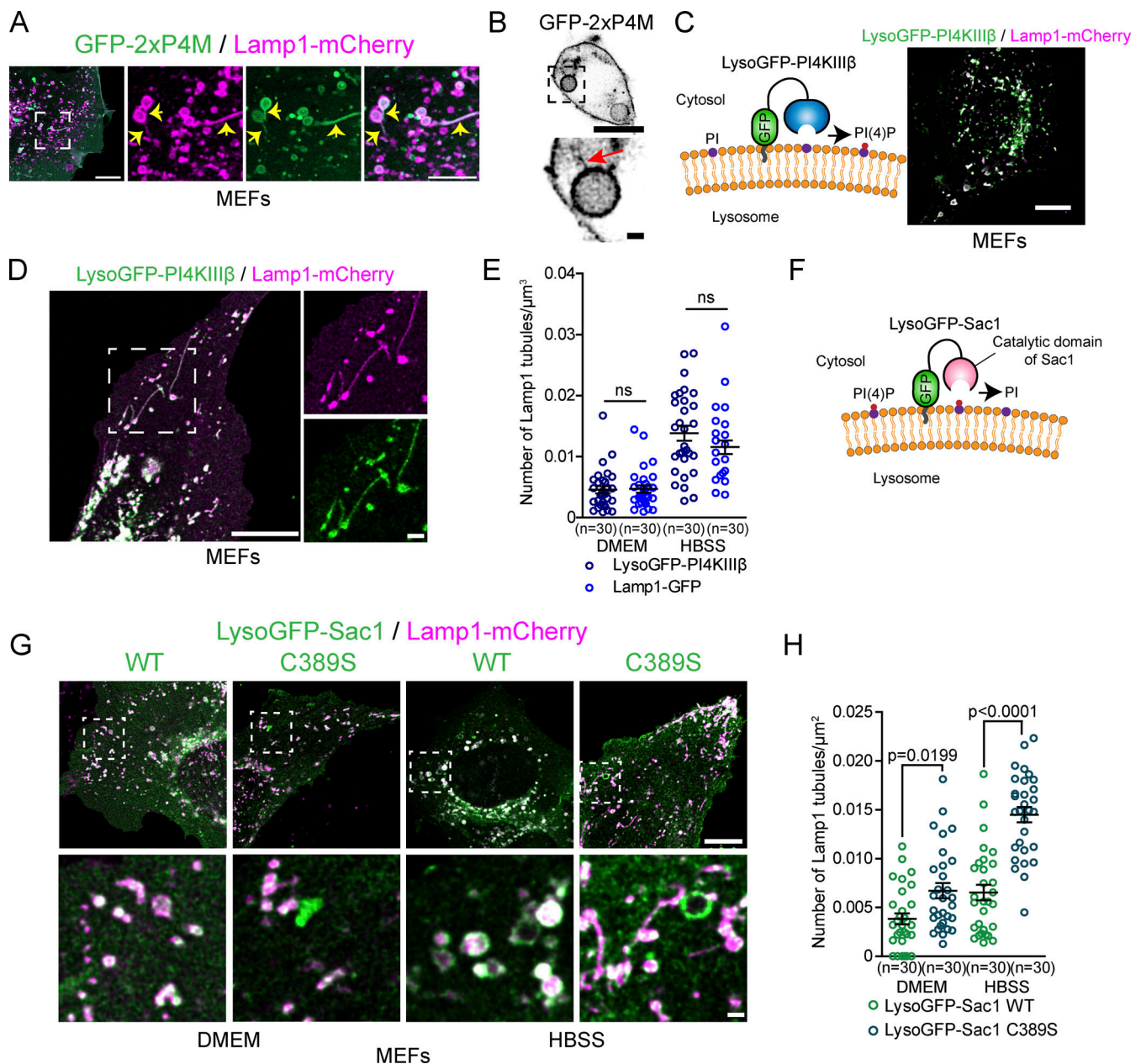
Figure 5. **PI(4)P has a pro-tubulation role at lysosomes. (A)** Representative images of Lamp1 positive tubules in MEFs expressing Lamp1-mCherry and the PI(4)P biosensor GFP-2xP4M after 8 h of starvation (HBSS). Lamp1 tubules are positive for 2xP4M. Scale bars: 10 and 5 μm (inset). **(B)** Representative images of a phagolysosome showing tubules positive for the PI(4)P biosensor GFP-2xP4M in RAW 264.7 macrophages phagocytosing SRBCs. Scale bars: 10 and 1 μm (inset). **(C)** LysoGFP-PI4KIIIβ fusion protein comprises PI(4)P producing enzyme PI4KIIIβ fused to the lysosomal targeting sequence of p18. LysoGFP-PI4KIIIβ colocalizes with Lamp1-mCherry in MEFs. Scale bars: 10 μm. **(D)** MEFs in HBSS show LysoGFP-PI4KIIIβ colocalized with Lamp1-mCherry positive tubules. Scale bar: 10 and 1 μm (inset). **(E)** Quantification of the number of Lamp1-mCherry positive tubules in MEFs expressing Lamp1-GFP or LysoGFP-PI4KIIIβ at basal state (DMEM) or 8H HBSS. The graphs show the mean ± SEM cells from three independent experiments. Two-way ANOVA with Tukey's multiple comparison test. ns: P = 0.9997 (DMEM) and P = 0.3093 (HBSS). **(F)** The PI(4)P phosphatase Sac1 was targeted to lysosomes by fusing it with the lysosomal targeting sequence of p18 to deplete lysosomes of PI(4)P. **(G)** Representative images of MEFs expressing LysoGFP-Sac1 wild-type (WT) or the catalytic dead (C389S) and Lamp1-mCherry at basal state (DMEM) or after prolonged starvation (HBSS, 8H). Scale bar: 10 and 1 μm (inset). **(H)** Quantification of the number of Lamp1 positive tubules in cells shown in G. The graphs show the mean ± SEM cells from three independent experiments. Two-way ANOVA with Tukey's multiple comparison test.

monitored PI(3)P levels on Lamp1 positive organelles undergoing tubule fission using the PI(3)P biosensor PX-p40phox (Wills et al., 2018; hereafter referred to as PX). We observed that Lamp1 tubule fission events were associated with an increase in PI(3)P levels in the seconds preceding the fission event (Fig. 6 A), while

there was no detectable increase on Lamp1 positive organelles with tubules that did not undergo fission (Fig. S7 A). A similar increase was observed using another PI(3)P biosensor (2xFYVE), but no change was observed for a PI(4)P biosensor (2xP4M; Fig. S7, B and C). These results indicate that the increase in PI(3)P
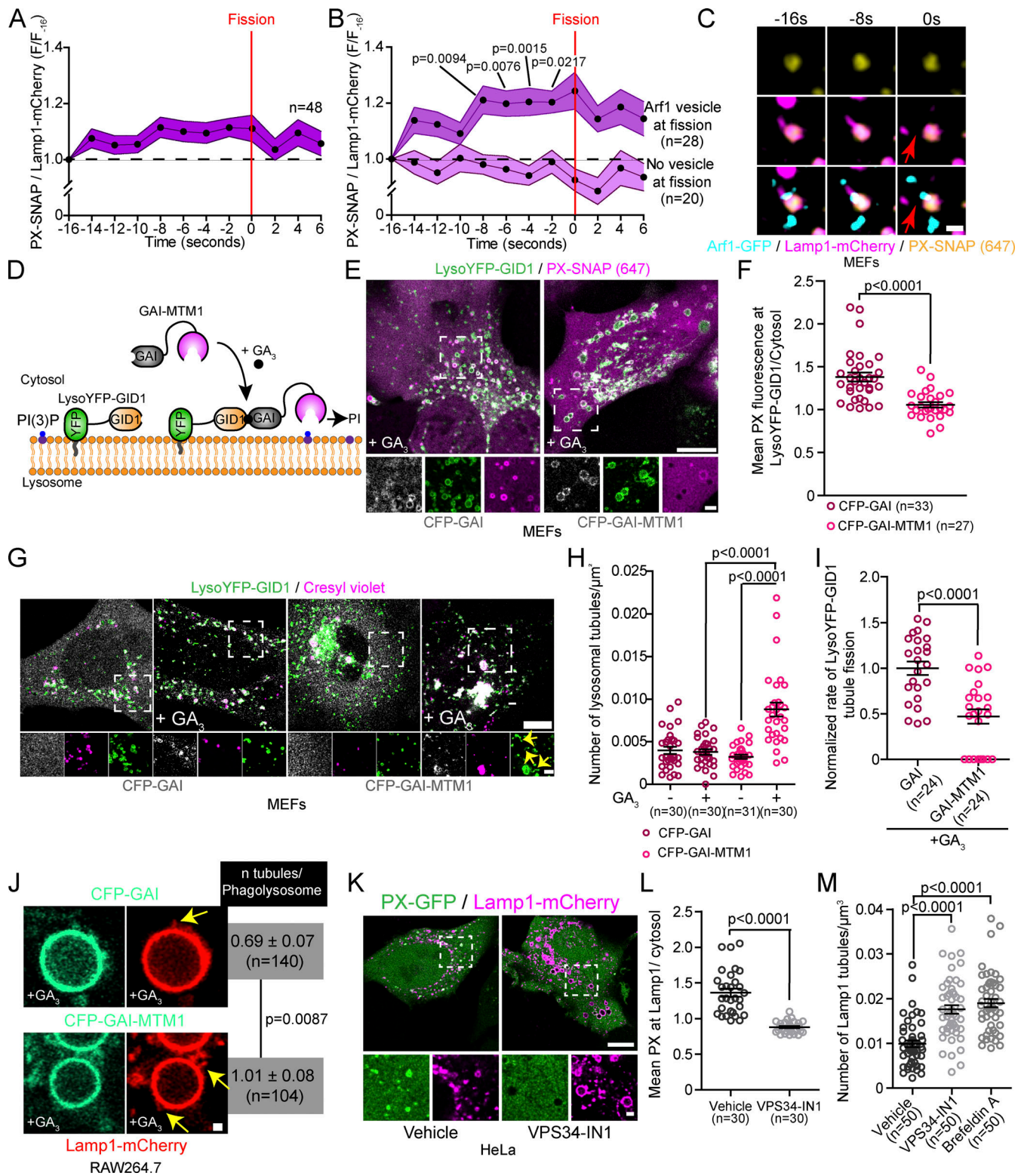
Figure 6. **Arf1 positive vesicle-mediated Lamp1 tubule fission events are associated with a PI(3)P increase and depletion of lysosomal PI(3)P impairs tubule fission. (A–C)** (A) Normalized fluorescence intensity of PX (PI(3)P biosensor) at Lamp1 positive organelles during tubule fission events. MEFs expressing Lamp1-mCherry treated with HBSS, 8 h. **(B)** Events monitored in A were classified according to the presence or absence of an Arf1 positive vesicle at the fission site. Two-way ANOVA with Tukey's multiple comparison test. **(C)** Representative time-lapse image of a Lamp1 fission event marked by an Arf1 positive vesicle analyzed in MEFs. Red arrows indicate fission. Scale bar: 1 μm. **(D)** Cartoon illustration of the GAI-GID1 dimerization system used to acutely recruit the PI(3)P phosphate MTM1 to lysosomes. **(E)** Representative Airyscan images of MEFs expressing LysoYFP-GID1, PX-SNAP, and CFP-GAI or CFP-GAI-MTM1 and treated with GA3-AM (10 μM for 1 h). Scale bar: 10 and 2 μm (insets). **(F)** Quantification of the mean fluorescence intensity of PX at LysoYFP-GID1 positive organelles normalized to cytosolic levels. Two-sided unpaired t test. **(G)** Representative Airyscan images of MEFs expressing LysoYFP-GID1 and CFP-GAI or CFP-GAI-

MTM1 before and after treatment with GA3-AM (10 µM for 1 h) and stained with the acidic marker Cresyl violet. Scale bars: 10 and 2 µm (inset). Yellow arrows indicate tubules. **(H)** Quantification of the number of lysosomal tubules in cells in G. Two-way ANOVA with Tukey's multiple comparison tests. **(I)** Normalized rate of tubule fission of LysoYFP-GID1 positive organelles after recruitment of indicated construct by GA3-AM treatment in starved MEFs (HBSS). Two-sided unpaired t test. **(J)** Representative Airyscan images of phagolysosomes from RAW 264.7 cells phagocyting SRBCs expressing iRFP-GID1-Rab7 (not imaged), Lamp1-mCherry, and CFP-GAI or CFP-GAI-MTM1 after treatment with GA3-AM (10 µM for 1 h; yellow arrows show tubules. Scale bar: 2 µm) and quantification of the number of tubules per phagolysosome. n = number of phagolysosomes. Two-sided unpaired t test. **(K–M)** Representative images of HeLa cells expressing Lamp1-mCherry and PX-GFP and treated with the VPS34 inhibitor VPS34-IN1 (1 µM for 1 h) or DMSO as vehicle control. Scale bar: 10 and 1 µm (inset). **(L)** Quantification of the levels of PX at Lamp1 positive organelles normalized to the cytosolic level of the probe. Two-sided unpaired t test. **(M)** Quantification of the number of Lamp1 positive tubules in these cells. BFA treatment (1 h) was used as a positive control. One-way ANOVA with Dunnett's multiple comparison test. All graphs (A, B, F, and H–M) show the mean ± SEM, cells from three independent experiments.

preceding fission is specific and not due to a general increase in phosphoinositide levels. The PI(3)P increase was also observed for tubule fission events from Lamp1 and overnight chased Dextran positive organelles, confirming that the fission of lysosomal tubules is associated with a PI(3)P increase (Fig. S7, D and E).

Next, to determine whether Arf1-PI4KIIIβ positive vesicles are required for the observed PI(3)P increase preceding fission, we classified the Lamp1 tubule fission events in Fig. 6 A based on the presence or absence of an Arf1 positive vesicle at the site of fission. We observed that the PI(3)P increase was only observed for the fission events marked by an Arf1 positive vesicle (Fig. 6, B and C), while the other events showed no detectable PI(3)P increase. Together, these results indicate that lysosomal tubule fission events marked by Arf1-PI4KIIIβ positive vesicles are associated with a PI(3)P increase in the seconds leading to fission.

Depletion of lysosomal PI(3)P impairs the fission of lysosomal tubules

Next, we asked whether PI(3)P is required for fission by acutely depleting PI(3)P on lysosomes by targeting the PI(3)P phosphatase MTM1 to lysosomes using the GAI-GID1 dimerization system (Miyamoto et al., 2012). We generated a construct where MTM1 was fused to GAI and co-expressed it with LysoYFP-GID1 (Lyso = lysosomal targeting sequence of p18) to target it to lysosomes (Fig. 6 D). Acute recruitment of MTM1, upon cell permeant GA$_3$-AM treatment that triggers GAI-GID1 dimerization, led to a striking decrease of the PI(3)P biosensor PX levels at LysoYFP-GID1 positive organelles (Fig. 6, E and F) and to a significant increase in the number of tubules emerging from acidic LysoYFP-GID1 positive organelles (Fig. 6, G and H) that was associated with a decrease in the rate of tubule fission from LysoYFP-GID1 positive organelles (Fig. 6 I). Similarly, the recruitment of GAI-MTM1 to phagolysosomes, using GID1-Rab7 as an anchor (Levin-Konigsberg et al., 2019), resulted in an increased number of tubules per phagolysosomes in RAW264.7 macrophages (Fig. 6 J). To confirm the importance of PI(3)P in the fission of lysosomal tubules, we inhibited the production of PI(3)P by VPS34, a PI3-kinase that notably produces PI(3)P at lysosomes (Munson et al., 2015), using the chemical inhibitor VPS34-IN1. This led to a strong depletion of PI(3)P levels at Lamp1 positive organelles and markedly increased the number of Lamp1 tubules in HeLa cells (Fig. 6, K–M), as previously reported (Munson et al., 2015), while it did not affect the number of Arf1 or PI4KIIIβ positive vesicles (Fig. S7, F–I). These results support that PI(3)P is required on lysosomes for tubule fission.

Collectively, these data suggest that Arf1-PI4KIIIβ positive vesicles mediate the increase in PI(3)P on the lysosome that drives the fission of their tubules.

The Arf1-PI4KIIIβ positive vesicle localized protein SEC14L2 contributes to the fission of lysosomal tubules

The PI(3)P signaling involved in Rab5 early endosome fission regulated by Arf1 positive vesicles were shown to be mediated by a protein called SEC14L2 (Gong et al., 2021). SEC14L2, which is found on Arf1 positive vesicles, is a lipid-binding protein that binds and transfers PI(3)P. SEC14L2 was proposed to regulate Rab5 early endosomes fission by either transferring PI(3)P from Arf1 vesicles to Rab5 endosomes or by activating the PI(3)P production machinery at the endosome-Arf1 vesicle contact site (Gong et al., 2021). Thus, we asked whether SEC14L2 could also contribute to the fission of lysosomal tubules mediated by Arf1-PI4KIIIβ positive vesicles. When overexpressed, SEC14L2 shows a diffuse cytosolic signal. However, removing excess cytosolic signal by permeabilizing the plasma membrane with digitonin before fixation showed colocalization of SEC14L2-mCherry to a subpopulation of Arf1-PI4KIIIβ positive vesicles in HeLa cells (Fig. 7 A), suggesting that SEC14L2 localizes to a subset of Arf1-PI4KIIIβ positive vesicles.

To assess whether SEC14L2 was required for lysosome tubule fission, we depleted the cells of endogenous SEC14L2 using siRNAs (Fig. 7 B). We found that depleting HeLa cells of SEC14L2 significantly increased the number of tubules from Lamp1 positive organelles compared to siRNA control-treated cells and at similar levels to BFA treatment (Fig. 7, C and D). Cresyl violet staining validated that increased Lamp1 tubules were lysosomal (Fig. 7, E and F). To check for potential off-target effects of the siRNA, we expressed the zebrafish homologue of human SEC14L2, zSec14l3 (Gong et al., 2021) and found that it rescued the increase in tubules induced by the knockdown (Fig. 7 G). A similar increase in tubulation caused by SEC14L2 knockdown was observed for invertase-treated sucrosomes (endolysosomes; Fig. 7, H and I).

To confirm that the increased number of lysosomal tubules in SEC14L2 depleted cells was caused by defective fission, we monitored the rate of tubule fission from Lamp1 positive organelle fission induced by prolonged starvation or YM201636 treatment and washout. In both cases, siRNA-mediated depletion of SEC14L2 caused a significant decrease in the rate of tubule fission (Fig. 7, J and K). Moreover, we observed that the percentage of Lamp1 tubule fission events marked by an Arf1 positive vesicle was reduced in HeLa cells depleted of SEC14L2
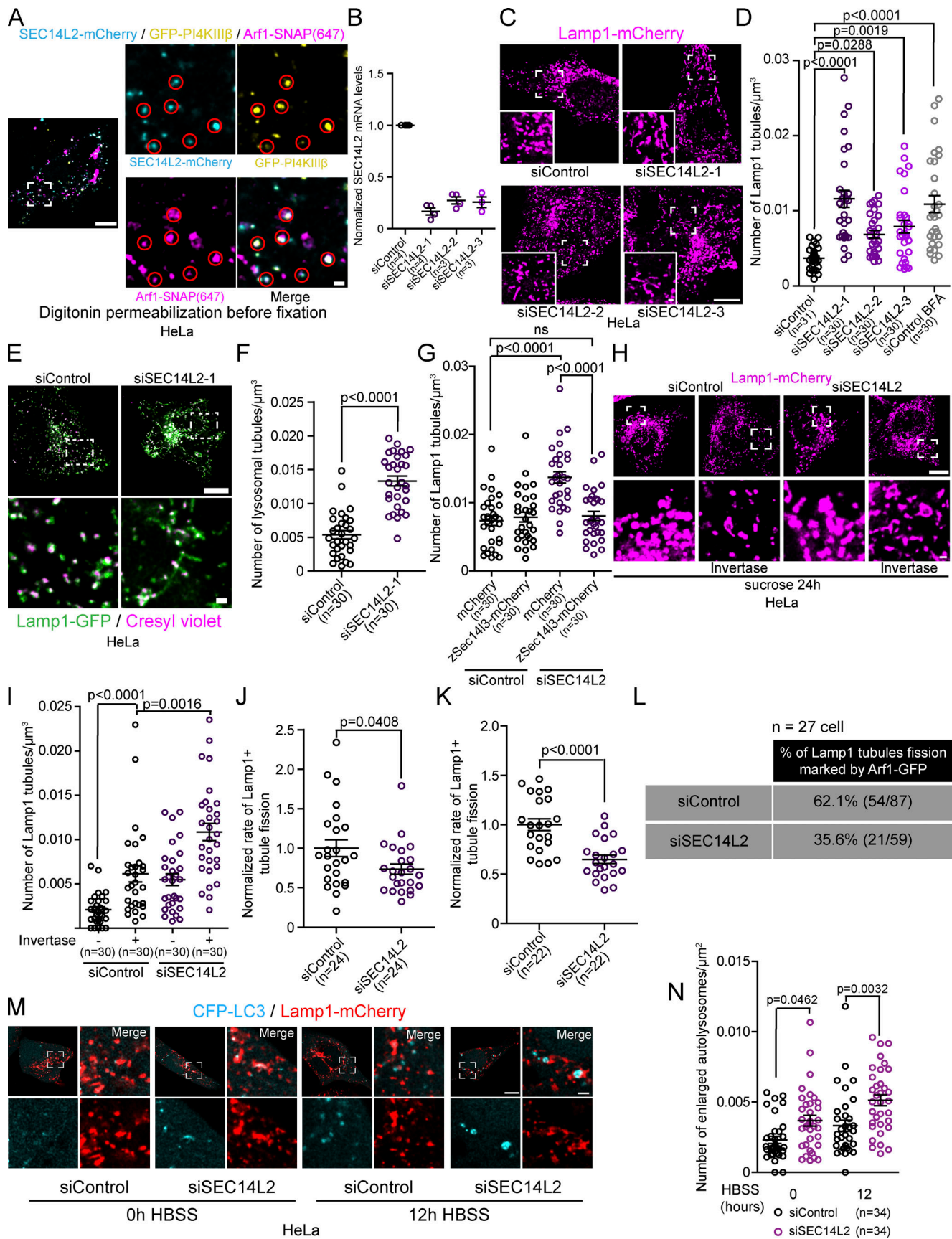
Figure 7. **The Arf1-PI4KIIIβ positive vesicle localized protein SEC14L2 contributes to the fission of lysosomal tubules. (A)** Representative image of a HeLa cell expressing SEC14L2-mCherry, GFP-PI4KIIIβ, and Arf1-SNAP. Excess cytosolic signal was removed by permeabilization with digitonin before fixation.

Boutry et al.
Lysosome tubules fission by Arf1-PI4KIIIβ vesicles

Journal of Cell Biology   13 of 23
https://doi.org/10.1083/jcb.202205128

Red circles show SEC14L2 colocalization with Arf1-PI4KIIIβ positive vesicles. Scale bar: 10 and 1 μm (inset). **(B)** Normalized SEC14L2 mRNA levels in cells treated with the indicated siRNAs. **(C and D)** Representative images of Lamp1 positive organelles morphology in HeLa cells expressing Lamp1-mCherry and treated with the indicated siRNAs (C) and quantification of the number of Lamp1 tubules in these cells (D). Scale bar: 10 and 1 μm (inset). BFA treatment (10 μg/ml for 1 h) was used as a positive control. One-way ANOVA with Dunnett's multiple comparison test. **(E and F)** Representative images of lysosomes (Cresyl violet positive Lamp1 organelles) in HeLa cells treated with the indicated siRNAs (E) and quantification of the number of lysosomal tubules (F). Scale bar: 10 and 1 μm (inset). Two-sided unpaired t test. **(G)** Quantification of the number of Lamp1 positive tubules in HeLa cells expressing cytosolic mCherry or the zebrafish SEC14L2 homologue zSec14l3-mCherry after treatment with the indicated siRNAs. Two-way ANOVA with Tukey's multiple comparisons test. ns: P value = 0.8998. **(H)** Representative images of HeLa cells treated with the indicated siRNAs and incubated with 30 mM sucrose for 24 h to promote the formation of endolysosomes (sucrosomes) before and after 2 h Invertase (0.5 mg/ml) as indicated. Scale bars: 10 and 1 μm (inset). **(I)** Quantification of the number of Lamp1 positive tubules in these cells in H. Two-way ANOVA with Tukey's multiple comparisons test. **(J and K)** Normalized rate of Lamp1 tubule fission in cells treated with the indicated siRNAs after prolonged starvation (HBSS 8 h; J) or 1 h inhibition of PIKfyve (YM201636) and washout of the drug (K). Two-sided unpaired t test. **(L)** Quantification of the number of Lamp1 tubule fission events marked by an Arf1 positive vesicle in cells treated with indicated siRNAs and starved (HBSS) for 8 h. **(M)** Representative images of cells expressing CFP-LC3 and Lamp1-mCherry treated with the indicated siRNAs and incubated in HBSS for the indicated time. Scale bars: 10 and 1 μm. **(N)** Quantification of the number of enlarged autolysosomes (>1 μm²) of cells in M. Two-way ANOVA with Tukey's multiple comparison tests. All graphs (B, D, F, G, I–K, and N) show the mean ± SEM, cells from three independent experiments.

compared to cells treated with a control siRNA (Fig. 7 L). Lastly, SEC14L2 depletion did not affect the formation of Arf1 or PI4KIIIβ positive vesicles (Fig. S7, J–M), suggesting that the decrease in fission events is not due to a loss of the Arf1-PI4KIIIβ vesicles. Taken together, our results support that SEC14L2, which localizes on Arf1-PI4KIIIβ positive vesicles, is required for the fission of lysosomal tubules.

Finally, since the formation and fission of autolysosomal tubules are required for clearance of enlarged autolysosomes after prolonged starvation (typically 12 h in HBSS; Rong et al., 2012), a defect in tubule fission would prevent the clearance of these enlarged autolysosomes. Thus, to confirm a role for SEC14L2 in the fission of lysosomal tubules, we monitored the number of enlarged autolysosomes in HeLa cells depleted of SEC14L2. We found that cells depleted of SEC14L2 had significantly more enlarged autolysosomes (>1 μm) after prolonged starvation compared to siRNA control-treated cells (Fig. 7, M and N). This result indicates that the knockdown of SEC14L2 impairs autophagic lysosome reformation and further supports that SEC14L2 is required fission of lysosomal tubules.

The PI(3)P binding domain of SEC14L2 is required for regulating lysosomal PI(3)P for lysosomal tubule fission

A key functional domain of SEC14L2 is its lipid binding CRAL-TRIO domain, which is required for binding and transferring PI(3)P (Gong et al., 2021). To test whether SEC14L2's lipid binding/transfer activity is required for lysosomal tubule fission, we performed complementation experiments by reintroducing various deleted constructs of zSec14l3 to HeLa cells depleted of its endogenous SEC14L2 with siRNA. Three different zSec14l3 mutants were used: (i) the previously described PI(3)P binding deficient mutant M5 (Gong et al., 2021); (ii) the ΔCRAL-TRIO construct that lacks the lipid binding domain; and (iii) the ΔGOLD construct lacking the Golgi dynamics (GOLD) domain of the protein (Fig. 8 A). We found that only the overexpression of wild-type zSec14l3 decreased the number of Lamp1 positive organelles tubules in cells depleted of SEC14L2 (Fig. 8 B). This strongly suggests that both its PI(3)P binding and GOLD domain are crucial for the fission of lysosomal tubules. Accordingly, the rate of tubule fission from Lamp1 positive organelles in HeLa cells depleted of SEC14L2, which is reduced compared to control cells

(Fig. 7 J), was increased by the expression of WT zSec14l3 but not by that of the PI(3)P binding deficient mutant M5 (Fig. 8 C).

Since we found SEC14L2 localized on Arf1-PI4KIIIβ positive vesicles and its PI(3)P binding domain was required for the efficient fission of tubules from Lamp1 positive organelles, a possible function for SEC14L2 during tubule fission may be to mediate the recruitment of Arf1-PI4KIIIβ positive vesicles to the site of lysosomal tubule fission by binding to lysosomal PI(3)P. To test this possibility, we monitored for the presence of Arf1 positive vesicles at Lamp1 positive organelle tubule necks, where we observed most fission events. We found that there was no difference in the percentage of Lamp1-positive organelle tubule necks showing contact with an Arf1 positive vesicle in SEC14L2-depleted cells compared to the control siRNA-treated cells (Fig. 8, D and E). This suggests that SEC14L2 has no role in the recruitment of Arf1-PI4KIIIβ positive vesicles to the site of lysosomal tubule fission. Similar results were observed in cells treated with the VPS34 inhibitor (Fig. 8 F), suggesting that an increase in lysosomal PI(3)P is not necessary for Arf1-PI4KIIIβ positive vesicle recruitment to fission sites.

Since we find that the PI(3)P binding ability of SEC14L2 is required for Lamp1 positive tubule fission and that lysosomal tubule fission events marked by an Arf1 positive vesicle are associated with an up-regulation of lysosomal PI(3)P levels, we reasoned that SEC14L2 could mediate the PI(3)P signaling required for tubule fission. Consistent with this hypothesis, depletion of SEC14L2 led to a decrease in the PI(3)P biosensor PX fluorescence at acidic lysosomes in resting cells, compared to cells treated with a control siRNA (Fig. 8, G and H). Importantly, the decrease in PI(3)P at lysosomes was rescued by the overexpression of wild-type zSec14l3 but not of the PI(3)P binding-deficient mutant M5 in cells where lysosomes were identified using overnight chased 10 kD Dextran (Fig. 8 I). These results support that SEC14L2 contributes to lysosomal tubule fission by regulating lysosomal PI(3)P levels.

Finally, SEC14L2 was shown to transfer PI(3)P and to promote PI(3)P production by activating VPS34 in vitro (Gong et al., 2021). Thus, we reasoned that if SEC14L2 regulates lysosomal PI(3)P to promote tubule fission by transferring it from Arf1-PI4KIIIβ positive vesicles or by activating VPS34 on lysosomes, the depletion of PI(3)P in the immediate proximity of SEC14L2 should impair tubule fission and leads to an increase in the
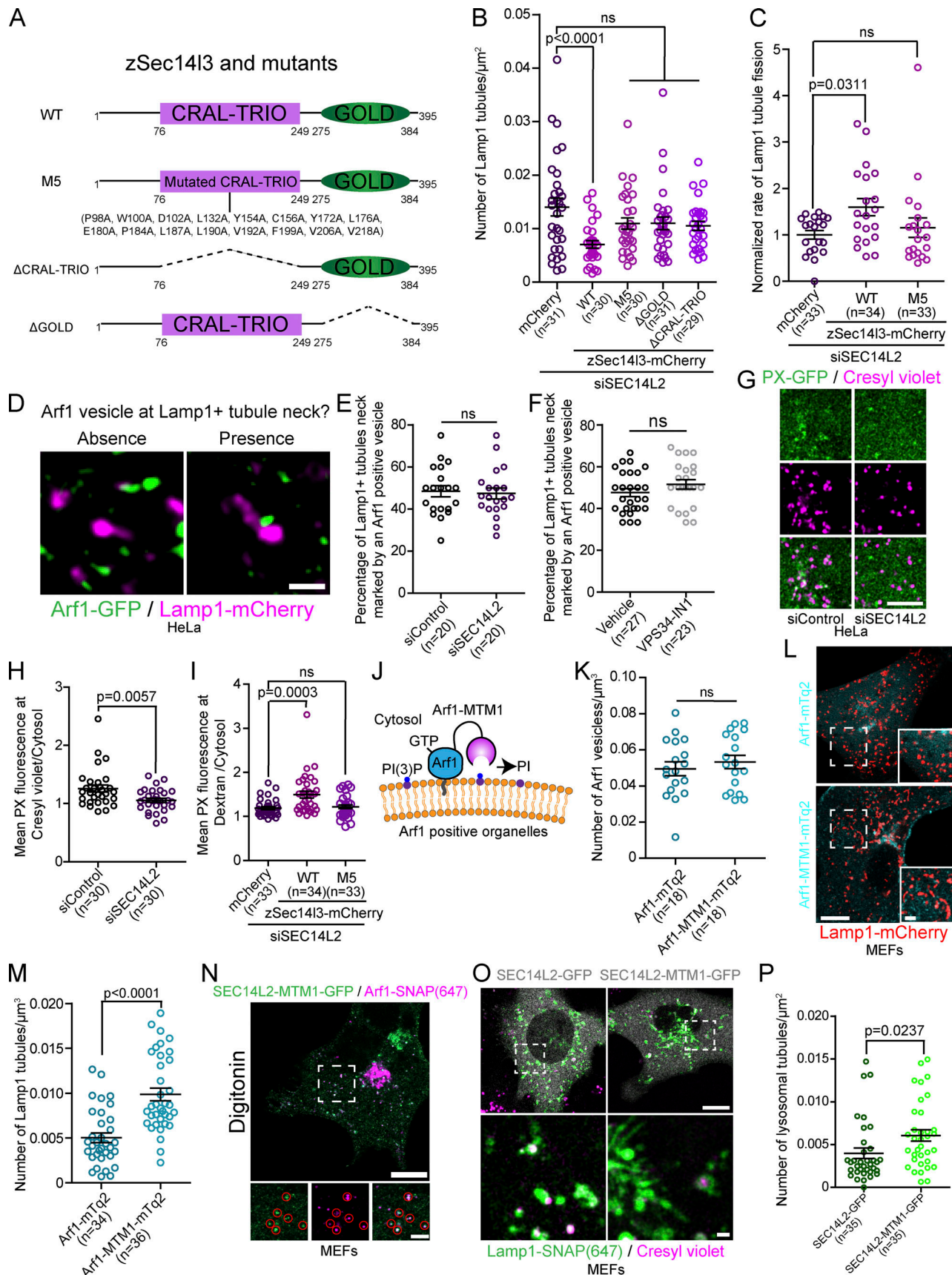
Figure 8. **The PI(3)P binding domain of SEC14L2 is required for regulating lysosomal PI(3)P and tubule fission. (A)** zSec14l3 constructs used in the study. **(B)** Quantification of the number of Lamp1 positive tubules in cells treated with the indicated siRNA and expressing the indicated constructs. One-way

ANOVA with Dunnett's multiple comparison test. P value = 0.1776 (M5), 0.1808 (ΔCRAL-TRIO), and 0.1069 (ΔGOLD). **(C)** Normalized rate of Lamp1 tubule fission in cells treated with the indicated siRNAs and expressing the indicated constructs. One-way ANOVA with Dunnett's multiple comparison test. ns = 0.7442. **(D–F)** Representative images showing the absence and presence of an Arf1 positive vesicle at Lamp1 positive organelle tubule necks. Scale bar: 1 µm (D). Quantification of the percentage of Lamp1 tubule necks marked by an Arf1 positive vesicle in cells treated with the indicated siRNA and starved (HBSS) for 8 h (E) or treated with VPS34-IN1 (1 µM for 1 h; F). Two-sided unpaired *t* test. ns: P value = 0.7773 (E) and 0.1825 (F). **(G)** Representative images of a 10 µm × 10 µm section of a cell treated with the indicated siRNA expressing PX-GFP. Acidic lysosomes were marked using cresyl violet Scale bar: 5 µm. **(H)** Quantification of the PX levels colocalizing with cresyl violet normalized to the cytosolic level of PX of cells in G. Two-sided unpaired *t* test. **(I)** Quantification of the PX levels colocalizing with overnight chased 10 kD Dextran normalized to the cytosolic level in cells treated with indicated siRNA and expressing the indicated constructs. One-way ANOVA with Dunnett's multiple comparison test. ns = 0.8898. **(J)** Cartoon illustration of the Arf1-MTM1 construct. **(K)** Quantification of the number of Arf1-GFP positive vesicles per cell in MEFs expressing Arf1-mTq2 or Arf1-MTM1-mTq2. Two-sided unpaired *t* test. ns: P value = 0.4901. **(L and M)** (L) Representative images of cells expressing Lamp1-mCherry and Arf1-mTq2 or Arf1-MTM1-mTq2; scale bar: 10 µm. (M) Quantification of the number of Lamp1 positive tubules in these cells. Two-sided unpaired *t* test. **(N)** Representative Airyscan image of a MEF cell expressing SEC14L2-MTM1-GFP and Arf1-SNAP. Red circles show SEC14L2-MTM1 colocalizing with Arf1 positive vesicles. Scale bar: 10 and 1 µm (inset). **(O and P)** Representative Airyscan images of MEFs expressing Lamp1-SNAP and SEC14L2-GFP or SEC14L2-MTM1-GFP and treated with Cresyl violet to mark acidic lysosomes (scale bar: 10 and 1 µm [inset]; O) and the quantification of the number of lysosomal tubules (P). Two-sided unpaired *t* test. All graphs (B, C, E, F, H, I, K, M, and P) show the mean ± SEM, cells from three independent experiments.

number of Lamp1 positive tubules. To test this, we first fused the PI(3)P phosphatase MTM1 to Arf1 (Fig. 8 J). Anchoring MTM1 to Arf1 did not affect the formation of Arf1 positive vesicles (Fig. 8 K) but led to an increased number of Lamp1 positive tubules in MEFs as compared to cells expressing Arf1-mTq2 that were used as a control (Fig. 8, L and M). Second, we fused MTM1 directly to SEC14L2, which did not impair the localization of SEC14L2 to Arf1 positive vesicles (Fig. 8 N) but did lead to an increase in the number of lysosomal tubules (Fig. 8, O and P). These results strengthen the link between SEC14L2 and PI(3)P in lysosomal tubule fission events as they support that depleting PI(3)P at the site of SEC14L2 localization or its immediate proximity impairs lysosomal tubule fission. Further, this result is consistent with a model where SEC14L2 regulates lysosomal PI(3)P levels to promote tubule fission by a transfer mechanism from Arf1-PI4KIIIβ positive vesicles or by activating VPS34 on lysosomes at contact sites with the vesicles. Collectively, our data suggest that Arf1-PI4KIIIβ positive vesicle localized SEC14L2 is required for the fission of lysosomal tubules by mediating a PI(3)P signaling on lysosomes.

Discussion

Formation and fission of lysosomal tubules allow for the re-generation of lysosomes from parent lysosomal organelles such as endolysosomes, autolysosomes, or phagolysosomes (Yang and Wang, 2021; Yu et al., 2010; Bright et al., 2016; Lancaster et al., 2021). However, the molecular mechanisms regulating these processes are only partially known. In this study, we used live-cell super-resolution imaging to investigate the role of Arf1-PI4KIIIβ positive vesicles in lysosomal tubule fission events. We observed that these vesicles are recruited to a broad range of lysosomal tubule fission events and that inactivation of Arf1 or inhibition of PI4KIIIβ impairs the fission of these tubules. Our study also suggest that Arf1-PI4KIIIβ positive vesicles mediate a PI(3)P signal at the site of fission through a SEC14L2-dependent mechanism. This mechanism involves SEC14L2 either mediating a PI(3)P transfer from the vesicle to the lysosome or activating lysosomal VPS34 at contact sites between the vesicle and the lysosome. Fig. 9 provides a visual representation of this pro-posed mechanism.

The vesicles that mark the site of lysosomal tubule fission are positive for the Golgi apparatus proteins Arf1, PI4KIIIβ, and TGN46, suggesting that these vesicles are derived from the Golgi. Similar Golgi protein positive vesicles were previously reported in the fission of endosomes (Gong et al., 2021) and mitochondria (Nagashima et al., 2020) and were termed Golgi-derived vesicles. However, we elected to call them Arf1-PI4KIIIβ positive vesicles since the markers used in our study are not restricted to the Golgi and Golgi-derived vesicles. For instance, both Arf1 and TGN46 have been shown on endosomes, albeit at low amounts (Nakai et al., 2013; Saint-Pol et al., 2004). Although these vesicles are unlikely to be endosomes as they are negative for common early and recycling endosomal markers such as Rab5, EEA1, and Rab11, it remains possible that these Arf1-PI4KIIIβ positive vesicles at the site of lysosomal tubule fission represent non-Golgi pools of Arf1, PI4KIIIβ, and TGN46. Further studies are required to determine the precise nature of these vesicles, including whether they represent Golgi-derived vesi-cles and whether they differ from the Arf1 positive vesicles regulating the fission of endosomes or mitochondria.

The recruitment of Arf1-PI4KIIIβ positive vesicles to fission sites likely involves various tethering factors allowing the es-tablishment of a membrane contact site between the vesicle, the lysosome and potentially the ER at the site of fission. Indeed, we observed that the ER marked the majority of Lamp1 tubule fis-sion sites suggesting a three-way contact between the three structures is involved. Multi-organelle interactions were re-cently identified in the division of mitochondria (Nagashima et al., 2020; Boutry and Kim, 2021) and endosomes (Gong et al., 2021), further suggesting that membrane fission events are highly coordinated processes requiring the involvement of multiple organelles. In all these cases, the ER appears to be the common organelle, thus supporting the idea that the ER may regulate contact between different organelles (Wenzel et al., 2022; Boutry and Kim, 2021).

A recent study reported that Arf1 positive Golgi-derived vesicles contribute to the division of endosomes by promoting an increase of PI(3)P on their membranes (Gong et al., 2021). We found that lysosomal tubule fission events marked by Arf1-PI4KIIIβ positive vesicles were similarly associated with an in-crease in PI(3)P levels on lysosomes in the seconds preceding
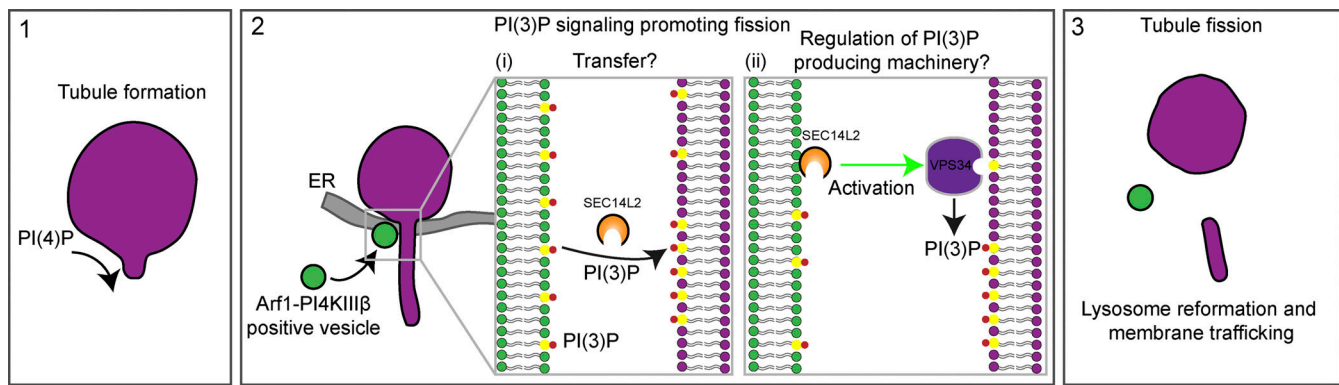
Figure 9. Proposed model for Arf1-PI4KIIIβ positive vesicles function at lysosomal tubules fission site. (1) Formation of lysosomal tubules from lysosomes, autolysosomes, endolysosomes, and phagolysosomes requires PI(4)P on the cytosolic leaflet of the lysosome membrane. **(2 i and ii)** Arf1-PI4KIIIβ positive vesicles are recruited to lysosomal tubule fission events, where the ER is also present. At these tri-organelle contact sites, we propose that SEC14L2 on the Arf1-PI4KIIIβ positive vesicle mediates a PI(3)P signal on the lysosomal membrane by (i) transferring PI(3)P from the vesicle to the lysosome, or (ii) regulating the activity of PI(3)P production machinery on lysosomes. These two mechanisms are not mutually exclusive. **(3)** PI(3)P signaling on tubules leads to fission of the tubule allowing for lysosome reformation from parent lysosome organelles (autolysosomes, endolysosomes, or phagolysosomes) or membrane trafficking events. Lysosomes are depicted in magenta, Arf1-PI4KIIIβ positive vesicles in green and the ER in gray.

fission. However, this increase in PI(3)P is unlikely to be required for recruiting the vesicle to the lysosomal tubule fission site since decreasing lysosomal PI(3)P levels by inhibiting VPS34 did not alter the recruitment of Arf1-PI4KIIIβ positive vesicles to Lamp1 positive tubule necks. Instead, this PI(3)P increase appears to be critical for fission event as the acute depletion of PI(3)P at organelles positive for the Lyso tag (P18 lysosomal anchoring N-terminus; Lim et al., 2019) markedly impaired the fission of lysosomal tubules. Collectively, these data suggest that Arf1-PI4KIIIβ positive vesicles mediate a PI(3)P signaling to drive the fission of lysosomal tubules.

We identified the PI(3)P binding protein SEC14L2 as a potential mediator of the increase of PI(3)P at the site of fission. SEC14L2 is a lipid-binding protein that was shown to bind and transfer PI(3)P in vitro and shown to contribute to the fission of Rab5 early endosomes (Gong et al., 2021). We find that SEC14L2 localizes to a subset of Arf1-PI4KIIIβ positive vesicles and is required for efficient fission of lysosomal tubules. Depleting SEC14L2 not only impaired the fission of tubules but also decreases PI(3)P levels on lysosomal organelles. Further, overexpression of wild-type zSec14l3, a zebrafish homologue of SEC14L2, but not of a PI(3)P binding-deficient mutant (zSec14l3-M5) increased both the PI(3)P levels and the tubule fission rate in SEC14L2 depleted cells. These findings support a model where the Arf1-PI4KIIIβ positive vesicle localized SEC14L2 regulates lysosomal PI(3)P to promote the fission of their tubules.

SEC14L2 may regulate PI(3)P at the site of lysosome tubule fission through different mechanisms (Fig. 9). One possible way is by transferring PI(3)P to lysosomes from Arf1-PI4KIIIβ positive vesicles. This is supported by recent reports that SEC14L2 can transport PI(3)P between liposomes (Gong et al., 2021), and our findings show that when we fuse the PI(3)P phosphatase MTM1 to SEC14L2 or Arf1, it increases the number of Lamp1 positive tubules. However, SEC14L2 may also increase PI(3)P on lysosomes by regulating its production, perhaps by binding to PI(3)P on lysosomes to activate VPS34. In favor of this model,

SEC14L2 was shown to activate VPS34 in vitro (Gong et al., 2021), and we and others (Munson et al., 2015) found that chemically inhibiting VPS34 impairs the fission of lysosomal tubules. These two models are not mutually exclusive and could work in synergy, perhaps providing a timed burst of PI(3)P at the site of fission. This could explain why Arf1-PI4KIIIβ positive vesicles are not recruited to all lysosomal tubule fission events. Finally, our results are consistent with a model where SEC14L2 would transfer phosphatidylinositol (PI) to lysosomes that would be used as a substrate by VPS34 to produce PI(3)P. However, as SEC14L2 binds weakly to PI compared to PI(3)P (Gong et al., 2021), this possibility appears least likely. The precise role of the PI(3)P signaling contributing to lysosomal tubule fission remains unresolved. However, as phosphoinositides can recruit specific proteins to membranes (Balla, 2013), it is tempting to speculate that PI(3)P could allow for the recruitment of effectors required for the scission of lysosomal tubules.

Finally, we found that PI(4)P is required for the formation of tubules from lysosomes and autolysosomes. Previously, PI(4)P production on lysosomes by PI4KIIIβ was proposed to inhibit the formation of lysosomal and autolysosomal tubules as inhibiting PI4KIIIβ caused lysosomal tubulation (Sridhar et al., 2013). However, we found that the production of PI(4)P on lysosomes does not impair their ability to tubulate, but instead that PI(4)P is required for tubulation as its depletion strongly suppresses the tubulation of lysosomes. This is in line with several studies showing that PI(4)P promotes the formation of tubules in the phagolysosomes (Levin-Konigsberg et al., 2019) and endosomes (Jani et al., 2022; Zhu et al., 2022; Jović et al., 2012). Our results indicate that the extensive tubulation of lysosomes caused by PI4KIIIβ inhibition is the result of impaired fission of lysosomal tubules. We propose that loss of PI4KIIIβ function affects the function and/or the formation of Arf1-PI4KIIIβ positive vesicles since PI4KIIIβ collaborates with Arf1 at the Golgi to promote the formation of vesicles from the trans-Golgi network (Waugh, 2019; Godi et al., 1999). Moreover, this increased number of

lysosomal tubules suggests that PI4KIIIβ does not play a major role in the production of PI(4)P required for lysosomal tubules formation and that type II PI4Ks, which were proposed to produce PI(4)P on lysosomes (Jović et al., 2012; Balla et al., 2002), are likely generating PI(4)P on lysosomes allowing membrane tubulation to occur. Further studies will be required to determine the source of PI(4)P required for lysosomal tubulation.

In summary, we propose that the formation and fission of lysosomal tubules required for lysosome reformation implicates an exquisite regulation of phosphoinositides levels on the lysosome membrane. We show that PI(4)P is required on lysosomes to generate tubules and that lysosomal PI(3)P is critical for the fission event. Our study supports that Arf1-PI4KIIIβ positive vesicles play a significant role in promoting SEC14L2-dependent PI(3)P signaling at the site of fission, leading to the fission of lysosomal tubules in a wide range of lysosomal organelles.

Materials and methods

Antibodies and chemicals
The following antibodies were used in this study: rabbit anti-LC3B (dilution: 1:1,000, NB100-2220; Novus biologicals), rabbit anti-β-Actin HRP conjugated (dilution 1:10,000, 5125; Cell signaling), rabbit anti-*E. coli* antibodies (1:100, 4329-4096; Bio-Rad), and goat anti-rabbit HRP (dilution: 1:10,000; 31460; Thermo Fisher Scientific). Brefeldin A (B7651), Invertase (I4504), Rapamycin (R0395), and Sucrose (S0389) were purchased from Sigma-Aldrich. Dynasore and PIK93 were purchased from Tocris. YM201636, ikarugamycin, Bafilomycin A1, and VPS34-IN1 were purchased from Cayman Chemicals. PI4KIIIbeta-IN-10 (HY-100198) was purchased from MedChemExpress. Sheep red blood cells (10% suspension) and rabbit anti-sheep antibodies (IgG fraction) were purchased from MP Biomedicals.

Plasmids
Unless otherwise stated, all plasmids encoding a fluorescent protein are monomerized versions in the Clontech N1 or C1 vectors. The following plasmids were used in this study: GFP-KDEL, CFP-LC3, mCherry-LC3, and ub-RFP-SKL were previously described (Kim et al., 2006; Wang et al., 2012). Lamp1-mCherry was a gift from Amy Palmer (University of Colorado Boulder, Boulder, CO, USA; #45147; Addgene); Arf1-GFP was a gift from Paul Melançon (University of Alberta, Edmonton, Canada; #39514; Addgene); TGN46-mEmerald was a gift from Michael Davidson (Florida State University, Tallahassee, FL, USA; #54279; Addgene); and mCherry-FKBP-MTM1 was a gift from Tamas Balla (National Institutes of Health, Bethesda, MD, USA; #51614; Addgene); the bacterial expression vector pBAD::mRFP1 was a gift from Robert Campbell (University of California at San Diego, La Jolla, CA, USA; #54667; Addgene). GFP-PI4KIIIβ (Levin et al., 2017), GFP-2xP4M (#51472; Addgene), mCherry-P4M (#51471; Addgene), PX-GFP (#19010; Addgene), GFP-2xFYVE (#140047; Addgene), iRFP-FRB-Rab7 (#51613; Addgene), GFP-Rab5 (#31733; Addgene), GFP-ORPSAC1 (Levin-Konigsberg et al., 2019), and GFP-EEA1 (#42307; Addgene) were a gift from Sergio Grinstein (The Hospital for Sick Children, Toronto, Canada). CFP-Rab11 was a gift from John Brumell (The Hospital for Sick

Children, Toronto, Canada), which was subcloned into the pECFP-C1 vector (Clontech) by excising Rab11b from EGFP-Rab11B with EcoR1 and XhoI (Smith et al., 2005). SEC14L2 human ORF (BC058915) was a gift from Brian Raught (Princess Margaret Cancer Centre, Toronto, Canada). Arf1-BFP was generated by replacing GFP with BFP (from mitoBFP #49151; Addgene, gift from William Trimble, The Hospital for Sick Children, Toronto, Canada). Arf1-MTM1-mTq2 was generated by inserting MTM1 from mCherry-FKBP-MTM1 in between Arf1 and mTq2 of Arf1-mTq2 that was made by replacing GFP from Arf1-GFP by mTq2 from mTq2-GAI-ORP1L (Levin-Konigsberg et al., 2019; gift from Sergio Grinstein, The Hospital for Sick Children, Toronto, Canada). SEC14L2-mCherry was made by replacing Lamp1 (in Lamp1-mCherry) with SEC14L2. SEC14L2-GFP was made by replacing Arf1 (in Arf1-GFP) with SEC14L2. SEC14L2-MTM1-GFP was generated by inserting MTM1 from mCherry-FKBP-MTM1 between SEC14L2 and GFP of SEC14L2-GFP. LysoGFP-Sac1 and LysoGFP-Sac1 C389S were made by subcloning LysoGFP-Sac1 from pLJM1-Lyso-FLAG-GFP-Sac1-Cat-WT (gift from Roberto Zoncu, University of California, Berkeley, CA, USA; #134645; Addgene) and pLJM1-Lyso-FLAG-GFP-Sac1-Cat-CS (gift from Roberto Zoncu, University of California, Berkeley, CA, USA; #134653; Addgene) in a Clontech vector. GFP-ORPSAC1 C392S was generated from GFP-ORPSAC1 by site-directed mutagenesis. Arf1-SNAP, Lamp1-SNAP, and PX-SNAP were made by replacing GFP (in Arf1-GFP), mCherry (in Lamp1-mCherry), and GFP (in PX-GFP) with SNAP from SNAP-Sec61b (gift from Gia Voeltz, University of Colorado Boulder, Boulder, CO, USA; #141152; Addgene). CFP-GAI-MTM1 was made by inserting MTM1 from mCherry-FKBP-MTM1 after GAI in CFP-GAI(1-92); gift from Takanari Inoue (Johns Hopkins University, Baltimore, MD, USA; #37307; Addgene) using SalI and BamhI restriction sites. LysoGFP-PI4KIIIβ was made by replacing GFP from GFP-PI4KIIIβ with LysoGFP from LysoGFP-Sac1 using AgeI and BsrGI restriction sites. LysoYFP-GID1 was made by replacing GFP-PI4KIIIβ from LysoGFP-PI4KIIIβ by YFP-GID1 from YFP-GID1 (gift from Takanari Inoue, Johns Hopkins University, Baltimore, MD, USA; #37305; Addgene). zSec14l3-mCherry (Gong et al., 2021) was a gift from Dr. Shunji Jia (Tsinghua University, Beijing, China). zSec14l3-ΔCRAL-TRIO-mCherry and zSec14l3-ΔGOLD-mCherry were generated by PCR-mediated deletion of the coding regions of the CRAL-TRIO (amino acid 76–249), and the GOLD (amino acid 275–384) domains, respectively. zSec14l3-M5 was custom synthesized (GeneScript). DNA sequences were verified by Sanger sequencing.

siRNAs
The following siRNAs were used: SEC14L2 (siSEC14L2-1: 5′-GCC GAAUCCAGAUGACUAUUU-3′; siSEC14L2-2: 5′-GUGGCCUAUAAC CUCAUCAAA-3′; siSEC14L2-3: 5′-CCGAAACACUGAAGCGUCUUU-3′). siRNAs were custom synthesized from Millipore Sigma, and MISSION siRNA Universal Negative Control #1 (Sigma-Aldrich) was used as a negative control.

Cell culture and transfection
COS-7, HeLa, MEFs, HEK293, and RAW 264.7 cells were obtained from ATCC and were cultured in DMEM (Gibco) supplemented with 10% FBS (Wisent) at 37°C in humidified air containing 5%

CO_2. Primary mouse macrophages were obtained and cultured as previously described (Lancaster et al., 2021). Transfection was performed using the Neon transfection system (Invitrogen) according to the manufacturer's instructions, using the following parameters: 1050V, 30 ms, and two pulses (COS-7); 1005V, 35 ms, and two pulses (HeLa); 1350V, and 30 ms, and one pulse (MEFs), 1150V, 20 ms, and two pulses (HEK 293); and 1680V, 20 ms, and one pulse (RAW 264.7). 5 μg of DNA for 0.5×10^6 cells (1×10^6 cells for RAW 264.7) was used, and cells were imaged or treated 24 h after transfection. A siRNA final concentration of 100 nM was used for silencing experiments, and cells were imaged or treated 48 h after transfection.

Fixed-cell imaging of phagosome resolution
RAW 264.7 cells were seeded at 20% confluence on #1.5 coverglass (Electron Microscopy Sciences) the day prior to phagosome fragmentation. Following the drug treatment and phagosome resolution, cells were fixed with 4% paraformaldehyde (Electron Microscopy Sciences) for 15 min, and then washed three times with Phosphate-Buffered Saline (PBS; Bio Basic, Inc.). External bacteria were labeled with rabbit anti-*E. coli* antibody followed by DyLight 488-conjugated anti-rabbit antibodies. Cells were then mounted on a slide using Dako Mounting Medium (Agilent). Images were acquired on a Quorum spinning disk system (Quorum) consisting of a Leica DMi8 microscope (Leica), an Andor Diskovery Multimodal Imaging system (Oxford Instruments), and an Andor Zyla 4.2 Megapixel sCMOS camera (Oxford Instruments) and controlled by Quorum Wave FX Powered by MetaMorph software (Quorum).

Live imaging
Most images were acquired on a Leica SP8 laser scanning confocal microscope equipped with a Lightning (deconvolution) module. Cells were grown in Lab-Tek chambers (Nunc) with a borosilicate glass bottom. Prior imaging, media was replaced, and cells were imaged in regular media or HBSS as indicated in the legends, using a Leica SP8 with a 63× glycerol immersion objective lens, 1.3 NA (Leica) in a temperature (37°C) and atmosphere (5% CO_2) controlled environment. Depending on the experiments, a single optical section or a z-stack of three to five steps with a step size ranging from 250 to 340 nm was acquired. The Las X software (Leica) was used to perform acquisition, and images were deconvoluted with the lightning module (Leica) using adaptative parameters. For lysosomal tubule fission events, a video of 1.5 min with one frame every 2 s was acquired.

Some images were acquired on a Zeiss LSM980 laser scanning confocal microscope equipped with an Airyscan 2 module, with a 63× oil immersion objective lens, 1.3 NA (Zeiss) in a temperature (37°C) and atmosphere (5% CO_2) controlled environment, in which case this is indicated in the text and/or legends. Zen 3.3 (Zeiss) software was used to perform the acquisition. Cells imaged were of similar low intensity to compare cells with similar levels of overexpression.

LLSM
A ZEISS Lattice Lightsheet 7 system was used for this study. Samples were grown and imaged in Lab-Tek chambers (Nunc)

in a temperature (37°C), CO_2 (5%), and humidity (70%) controlled environment. Samples were illuminated by optical light sheets generated by beam shaping by cylinder lens and spatial light modulator (SLM) with beams of 30 μm in length and 1,000 nm of thickness using 488 and 561 nm lasers and appropriate filters. Fluorescent emission was collected by a detection objective (lens 44.83×/1.0 [at 60° angle to cover glass]) and a Pco.edge 4.2 CLHS sCMOS camera (6.5 μm pixel size, 2,048 × 2,048, 82% QE). Acquired data were deconvoluted (constrained iteration using automatic strength) and deskewed using Zen 3.3 software (Zeiss).

3D reconstruction
3D reconstructions of fluorescent images were performed using Imaris Bitplane (9.2.1) using the "Make surface" feature with default parameters.

Gibberellin-induced dimerization system
For Gibberellin-induced dimerization experiments, GID1-tagged membrane anchor proteins were used to recruit GAI-fused cytosolic construct upon GA_3-AM treatment (10 μM). Cells were imaged after 1 h of GA_3-AM treatment unless indicated in the text and/or legend.

Image analysis
The number of lysosomal tubules per cell was counted manually using ImageJ software, normalized to the volume or area of cells and expressed as "Number of Lamp1 tubules/μm³" or "Number of Lamp1 tubules/μm²." For lysosomes-Arf1 positive vesicle contact evaluation, the number of lysosomes showing contact with at least one Arf1 vesicle at one time frame was counted and was then expressed as a percentage. The minimum duration of contacts between these two compartments was analyzed as previously described (Boutry and Kim, 2021). Briefly, 10 randomly chosen contacts were analyzed. Only contacts that were already formed at the beginning of the acquisition and that lasted for at least three consecutive frames (>6 s) were analyzed. The minimum duration of contact was quantified as the time before the dissociation of the lysosome-Golgi-derived vesicle contact over a 1.5-min video. Contacts that lasted during the totality of the video were scored as 1.5-min (90-s) contacts.

Lamp1 positive organelles and Lysosomal tubule fission events were defined as events showing a clear division of a tubule from one Lamp1 positive organelle or from one parent lysosome organelle (autolysosome, endolysosome, or phagolysosome). In most cases (>90%), the fission event was observed at the tubule neck. However, fission events occurring in the middle of the tubules were also counted as positive. The presence of vesicle markers such as Arf1-GFP at the tubule fission site was defined as the contact of the vesicle with the tubule fission site at the frame just before the fission event was observed. The presence of vesicle markers at the fission site was then expressed as a percentage. To compare the percentage of fission sites marked by these vesicle markers to that of one expected by chance, we performed the same analysis, but after the Lamp1-mCherry channel was rotated by 90°. For the rate of Lamp1 tubule fission, the number of Lamp1

tubule fission events was counted and then normalized by time and volume to calculate a fission rate (normalized rate of Lamp1 tubule fission).

For phagosome resolution/fragmentation, images were converted to binary images. The intensity threshold for binary conversion was selected manually to preserve as many vesicular structures as possible while minimizing the merging of objects after binary conversion. This was then applied to all images across a biological replicate. Whenever necessary, the watershed function was used to further segment particles on the binary images. Phagosome fragments were counted using ImageJ's "Analyze particles" function. Fragments were defined as objects with an area between 10 and 1,000 pixels (0.04–3.83 µm²). Intact phagosomes and external particles were manually subtracted from the count. Fragments from whole cells were included in the analysis, while we excluded regions where cells were overly crowded, making dissection difficult. Fragments per cell were then quantified.

To estimate the levels of PI(3)P at lysosomes, the PI(3)P probe PX (Wills et al., 2018) was used. A mask of lysosomes (using cresyl violet or overnight chased 10 kD Dextran 647) was generated using an automatic threshold of ImageJ, and the mean fluorescent intensity of PX was measured. This was normalized to the cytosolic levels of PX. To evaluate whether the fission of Lamp1 tubules was associated with a regulation of PI(3)P and PI(4)P, we identified Lamp1 tubules fission events and measured these phosphoinositides using appropriate fluorescent biosensors (PX and 2xFYVE for PI(3)P; 2xP4M for PI(4)P) for eight frames (16 s) before the fission event and three frames (6 s) after it was observed. The fluorescence intensity was only measured on the Lamp1 positive organelle main body and tubule neck. The mean fluorescence intensity of the biosensor was normalized to that of Lamp1-mCherry for each respective frame. Enlarged autolysosomes were defined as Lamp1 and LC3 positive structures of more than 1 µm in diameter. The number of peroxisomes per cell was counted using Volocity software (Perkin Elmer) and was normalized to the volume of the cells.

Whenever possible, we performed a blind analysis of our data. After image acquisition, files were anonymized before analysis.

Quantitative PCR and primers
The Monarch Total RNA Miniprep Kit (New England BioLabs) was used to perform total cellular RNAs isolation, following manufacturer instructions, and cDNAs were subsequently synthesized using the High-Capacity cDNA Reverse Transcription kit (Applied Biosystems). qPCR was performed using a StepOne Real-Time PCR System using SYBR green (Thermo Fisher Scientific) using β-actin as a reference gene for all quantifications. The following primers were used: β-actin F: 5′-TGGCATCGTGAT GGACTCC-3′, β-actin R: 5′-AATGTCACGCACGATTTCCC-3′, SEC14L2 F: 5′-GGACGAGTCTGTGCTCCATC-3′ and SEC14L2 R: 5′-GACATTCTCCCGAAACTTGGC-3′.

Induced lysosomal tubule fission
Lysosomal tubule fission was promoted using four different ways: (1) by incubating cells for 8 h in an amino acid-free media

HBSS that triggers autophagic lysosome reformation which implicates formation of tubules from autolysosomes and their fission; (2) by reversibly inducing lysosomal swelling by incubating cells with 30 mM sucrose for 24 h, that leads to the formation of sucrosomes (swollen lysosomes full of sucrose). Mammalian cells cannot degrade sucrose which builds up in lysosomes leading to the formation of sucrosomes. Cells were then incubated with Invertase (0.5 mg/ml) for 1 h, allowing its endocytosis and delivery to lysosomes leading to sucrose degradation and subsequent lysosomal shrinkage in a process involving strong lysosomal fission; (3) by inducing phagolysosomes formation in RAW 264.7 macrophages by incubating cells with opsonized SRBCs; and (4) by reversibly inhibiting PIKFyve with YM201636 (1 µM for 1-h treatment) which leads to extensive lysosomal swelling. Upon washout of the drug (two subsequent washing with regular culture media), lysosomes shrink to return to their normal size in a process that involves strong lysosomal fission.

Phagocytosis
For phagocytosis experiments (except for phagosome fragmentation assay), opsonized sheep red blood cells (SRBCs) were used as prey for RAW264.7 macrophages. For opsonization, 100 µl of 20% SRBCs suspension was washed with PBS and opsonized with 3 µl of rabbit IgG fraction against SRBC for 1 h at 37°C under agitation. SRBCs were then washed twice with PBS and resuspended in 1,000 µl of PBS. Phagocytosis was induced by incubating cells with a 100-fold dilution of opsonized SRBCs suspension in regular media. Phagocytosis was synchronized by centrifuging the imaging chamber for 10 s at 300 g. Cells were then washed with HBSS and were imaged in HBSS.

Phagosome fragmentation assay
The assay was performed as previously described (Lancaster et al., 2021). In brief, fluorescently labeled *E. coli* (DH5α *E. coli* strain) were transformed with the pBAD::mRFP1 plasmid (Campbell et al., 2002), and RAW 264.7 were allowed to internalize mRFP1-labeled *E. coli*. Cells were then washed with regular media and incubated for the indicated time. Cells were treated with DMSO, 10 µM PIK93, 10 µM Brefeldin A (BFA), or 0.5 µg/ml Ikarugamycin (Ika) 1 h after phagocytosis and imaged after 5 h of treatment using a spinning disk confocal microscope.

Western blotting
Cells were lysed in a Lysis buffer (100 mM Tris-HCL, 1% SDS) containing a protease inhibitor cocktail (BioShop). Lysates were then incubated for 15 min at 95°C and vortexed briefly every 5 min during this incubation. Lysates were then centrifuged at 21,000 g for 15 min at room temperature. The supernatant was then collected, and their protein concentration was determined using the BCA assay kit (Thermo Fisher Scientific). Lysates were separated by SDS-PAGE and immunoblotted onto a PVDF membrane (Immobilon-PSQ; Millipore Sigma). Blocking was performed by incubating membranes in PBS Buffer 1X with 0.1% Tween 20 (#TWN510; BioShop) for 2 h at room temperature. Antibody incubation was done overnight in PBS Buffer 1X with 0.1% Tween 20 at 4°C. A ChemiDoc (Bio-Rad Laboratories) system was used to visualize proteins.

Labeling of lysosomes with Cresyl violet and fluorescent Dextran

Cresyl Violet (Sigma-Aldrich) staining was used to label acidic lysosomes (Ostrowski et al., 2016). Cells were incubated with 1 µM of Cresyl violet in HBSS for 3 min at 37°C, were then rinsed twice and incubated in appropriate media for imaging.

Alternatively, lysosomes were also stained using fluorescent 10 kD Dextran A647 (D22914; Thermo Fisher Scientific). Cells were incubated with 0.1 mg/ml of Dextran for 3 h at 37°C. Cells were then rinsed twice and chased overnight in appropriate media to allow the Dextran to reach lysosomes before imaging.

SNAP-tag labeling

To label SNAP tag-containing constructs, cells were incubated for 30 min at 37°C in appropriate media containing 3 µM of cell-permeable SNAP-Cell 647-SiR (catalog #S9102S; New England BioLabs). Cells were then rinsed twice with fresh media and incubated for 30 min at 37°C. Media was then replaced, and cells were imaged.

Graphing and figure assembly

Graphics were prepared using GraphPad Prism 5 or 9.3. The brightness and contrast of microscopy images were adjusted using ImageJ software for presentation purposes. For the experiment with constructs exhibiting a strong cytosolic signal (Arf1-GFP, Arf1-BFP, Arf1-SNAP, PX-SNAP, and GFP-PI4KIIIB), brightness and contrast were adjusted to mask the cytosolic signal allowing better visualization of vesicles, for presentation purposes. All final figures were assembled using Illustrator CS6 (Adobe).

Statistics and reproducibility

All statistical tests were performed using GraphPad Prism 5 and 9 and are described in the figure legends. Data distribution was assumed to be normal, but this was not formally tested. A P value of $P < 0.05$ was considered statistically significant. All Graphs show the mean ± SEM from three independent trials (unless specified in the legends).

Online supplemental material

Fig. S1 shows contacts between Arf1 vesicles and Lamp1 positive organelles and the presence of Arf1 vesicles at Lamp1 tubule fission events in HeLa cells. Fig. S2 shows the presence of the ER and the absence of peroxisomes at Lamp1 tubule fission events as well as the presence of PI4KIIIβ positive vesicles at Lamp1 tubule fission events from endolysosomes and phagolysosomes. Fig. S3 shows the control that the YM201636 treatment used in the study does not lead to the formation of endolysosomes or induction of autophagy. Fig. S4 shows the effect of PI4KIIIbeta-IN-10 or Brefeldin A treatment on the number of Arf1 or PI4KIIIβ positive vesicles in MEFs and on the number of lysosomal tubules in different cell lines. Fig. S5 shows that Brefeldin A treatment does not compromise phagolysosome fragmentation or the fission of vesicles from Lamp1 positive organelles. Fig. S6 shows validation of various methods used to modulate lysosomal PI(4)P levels and the control that depletion of lysosomal PI(4)P does not appear to compromise autophagosome-lysosome fusion. Fig. S7 shows quantifications of PI(3)P and PI(3)P on Lamp1 positive organelles showing tubule fission and quantification of the number of Arf1 or PI4KIIIβ positive vesicles after VPS34-IN1 treatment or SEC14L2 depletion. The sequence of primers used for cloning is indicated in Table S1. Video 1 shows that Arf1 positive vesicles and Lamp1 positive organelles appear to form dynamic contacts. Video 2 shows that Arf1 positive vesicles are recruited to Lamp1 positive tubule fission sites. Video 3 shows that Arf1 positive vesicles are recruited to sites of autolysosomal tubule fission. Video 4 shows that Arf1 positive vesicles are recruited to sites of phagolysosomal tubule fission.

Data availability

All data are available from the corresponding authors upon request.

References

Aranovich, A., R. Hua, A.D. Rutenberg, and P.K. Kim. 2014. PEX16 contributes to peroxisome maintenance by constantly trafficking PEX3 via the ER. *J. Cell Sci.* 127:3675–3686. https://doi.org/10.1242/jcs.146282

Baba, T., D.J. Toth, N. Sengupta, Y.J. Kim, and T. Balla. 2019. Phosphatidylinositol 4,5-bisphosphate controls Rab7 and PLEKHM1 membrane cycling during autophagosome-lysosome fusion. *EMBO J.* 38:e100312. https://doi.org/10.15252/embj.2018100312

Balla, A., G. Tuymetova, M. Barshishat, M. Geiszt, and T. Balla. 2002. Characterization of type II phosphatidylinositol 4-kinase isoforms reveals association of the enzymes with endosomal vesicular compartments. *J. Biol. Chem.* 277:20041–20050. https://doi.org/10.1074/jbc.M111807200

Balla, T. 2013. Phosphoinositides: Tiny lipids with giant impact on cell regulation. *Physiol. Rev.* 93:1019–1137. https://doi.org/10.1152/physrev.00028.2012

Bissig, C., I. Hurbain, G. Raposo, and G. van Niel. 2017. PIKfyve activity regulates reformation of terminal storage lysosomes from endolysosomes. *Traffic.* 18:747–757. https://doi.org/10.1111/tra.12525

Boutry, M., and P.K. Kim. 2021. ORP1L mediated PI(4)P signaling at ER-lysosome-mitochondrion three-way contact contributes to mitochondrial division. *Nat. Commun.* 12:5354. https://doi.org/10.1038/s41467-021-25621-4

Bright, N.A., L.J. Davis, and J.P. Luzio. 2016. Endolysosomes are the principal intracellular sites of acid hydrolase activity. *Curr. Biol.* 26:2233–2245. https://doi.org/10.1016/j.cub.2016.06.046

Campbell, R.E., O. Tour, A.E. Palmer, P.A. Steinbach, G.S. Baird, D.A. Zacharias, and R.Y. Tsien. 2002. A monomeric red fluorescent protein. *Proc. Natl. Acad. Sci. USA.* 99:7877–7882. https://doi.org/10.1073/pnas.082243699

Chang, J., S. Lee, and C. Blackstone. 2014. Spastic paraplegia proteins spastizin and spatacsin mediate autophagic lysosome reformation. *J. Clin. Invest.* 124:5249–5262. https://doi.org/10.1172/JCI77598

Choy, C.H., G. Saffi, M.A. Gray, C. Wallace, R.M. Dayam, Z.A. Ou, G. Lenk, R. Puertollano, S.C. Watkins, and R.J. Botelho. 2018. Lysosome enlargement during inhibition of the lipid kinase PIKfyve proceeds through lysosome coalescence. *J. Cell Sci.* 131:jcs213587. https://doi.org/10.1242/jcs.213587

Costello, J.L., I.G. Castro, C. Hacker, T.A. Schrader, J. Metz, D. Zeuschner, A.S. Azadi, L.F. Godinho, V. Costina, P. Findeisen, et al. 2017. ACBD5 and VAPB mediate membrane associations between peroxisomes and the ER. *J. Cell Biol.* 216:331–342. https://doi.org/10.1083/jcb.201607055

Crivelli, S.M., C. Giovagnoni, Z. Zhu, P. Tripathi, A. Elsherbini, Z. Quadri, J. Pu, L. Zhang, B. Ferko, D. Berkes, et al. 2022. Function of ceramide transfer protein for biogenesis and sphingolipid composition of extracellular vesicles. *J. Extracell. Vesicles.* 11:e12233. https://doi.org/10.1002/jev2.12233

Elkin, S.R., A.M. Lakoduk, and S.L. Schmid. 2016. Endocytic pathways and endosomal trafficking: A primer. *Wien. Med. Wochenschr.* 166:196–204. https://doi.org/10.1007/s10354-016-0432-7

Eskelinen, E.-L. 2006. Roles of LAMP-1 and LAMP-2 in lysosome biogenesis and autophagy. *Mol. Aspects Med.* 27:495–502. https://doi.org/10.1016/j.mam.2006.08.005

Eskelinen, E.-L., Y. Tanaka, and P. Saftig. 2003. At the acidic edge: Emerging functions for lysosomal membrane proteins. *Trends Cell Biol.* 13:137–145. https://doi.org/10.1016/s0962-8924(03)00005-9

Germain, K., and P.K. Kim. 2020. Pexophagy: A model for selective autophagy. *Int. J. Mol. Sci.* 21:E578. https://doi.org/10.3390/ijms21020578

Godi, A., P. Pertile, R. Meyers, P. Marra, G. Di Tullio, C. Iurisci, A. Luini, D. Corda, and M.A. De Matteis. 1999. ARF mediates recruitment of PtdIns-4-OH kinase-beta and stimulates synthesis of PtdIns(4,5)P2 on the Golgi complex. *Nat. Cell Biol.* 1:280–287. https://doi.org/10.1038/12993

Gong, B., Y. Guo, S. Ding, X. Liu, A. Meng, D. Li, and S. Jia. 2021. A Golgi-derived vesicle potentiates PtdIns4P to PtdIns3P conversion for endosome fission. *Nat. Cell Biol.* 23:782–795. https://doi.org/10.1038/s41556-021-00704-y

Hammond, G.R.V., M.P. Machner, and T. Balla. 2014. A novel probe for phosphatidylinositol 4-phosphate reveals multiple pools beyond the Golgi. *J. Cell Biol.* 205:113–126. https://doi.org/10.1083/jcb.201312072

Hoyer, M.J., P.J. Chitwood, C.C. Ebmeier, J.F. Striepen, R.Z. Qi, W.M. Old, and G.K. Voeltz. 2018. A novel class of ER membrane proteins regulates ER-associated endosome fission. *Cell.* 175:254–265.e14. https://doi.org/10.1016/j.cell.2018.08.030

Hua, R., D. Cheng, É. Coyaud, S. Freeman, E. Di Pietro, Y. Wang, A. Vissa, C.M. Yip, G.D. Fairn, N. Braverman, et al. 2017. VAPs and ACBD5 tether peroxisomes to the ER for peroxisome maintenance and lipid homeostasis. *J. Cell Biol.* 216:367–377. https://doi.org/10.1083/jcb.201608128

Jani, R.A., A. Di Cicco, T. Keren-Kaplan, S. Vale-Costa, D. Hamaoui, I. Hurbain, F.-C. Tsai, M. Di Marco, A.-S. Macé, Y. Zhu, et al. 2022. PI4P and BLOC-1 remodel endosomal membranes into tubules. *J. Cell Biol.* 221:e202110132. https://doi.org/10.1083/jcb.202110132

Johnson, D.E., P. Ostrowski, V. Jaumouillé, and S. Grinstein. 2016. The position of lysosomes within the cell determines their luminal pH. *J. Cell Biol.* 212:677–692. https://doi.org/10.1083/jcb.201507112

Jović, M., M.J. Kean, Z. Szentpetery, G. Polevoy, A.-C. Gingras, J.A. Brill, and T. Balla. 2012. Two phosphatidylinositol 4-kinases control lysosomal delivery of the Gaucher disease enzyme, β-glucocerebrosidase. *Mol. Biol. Cell.* 23:1533–1545. https://doi.org/10.1091/mbc.e11-06-0553

Kim, P.K., R.T. Mullen, U. Schumann, and J. Lippincott-Schwartz. 2006. The origin and maintenance of mammalian peroxisomes involves a de novo PEX16-dependent pathway from the ER. *J. Cell Biol.* 173:521–532. https://doi.org/10.1083/jcb.200601036

Lancaster, C.E., A. Fountain, R.M. Dayam, E. Somerville, J. Sheth, V. Jacobelli, A. Somerville, M.R. Terebiznik, and R.J. Botelho. 2021. Phagosome resolution regenerates lysosomes and maintains the degradative capacity in phagocytes. *J. Cell Biol.* 220:e202005072. https://doi.org/10.1083/jcb.202005072

Levin, R., G.R.V. Hammond, T. Balla, P. De Camilli, G.D. Fairn, and S. Grinstein. 2017. Multiphasic dynamics of phosphatidylinositol 4-phosphate during phagocytosis. *Mol. Biol. Cell.* 28:128–140. https://doi.org/10.1091/mbc.e16-06-0451

Levin-Konigsberg, R., F. Montaño-Rendón, T. Keren-Kaplan, R. Li, B. Ego, S. Mylvaganam, J.E. DiCiccio, W.S. Trimble, M.C. Bassik, J.S. Bonifacino, et al. 2019. Phagolysosome resolution requires contacts with the endoplasmic reticulum and phosphatidylinositol-4-phosphate signalling. *Nat. Cell Biol.* 21:1234–1247. https://doi.org/10.1038/s41556-019-0394-2

Lim, C.-Y., O.B. Davis, H.R. Shin, J. Zhang, C.A. Berdan, X. Jiang, J.L. Counihan, D.S. Ory, D.K. Nomura, and R. Zoncu. 2019. ER-lysosome contacts enable cholesterol sensing by mTORC1 and drive aberrant growth signalling in Niemann-Pick type C. *Nat. Cell Biol.* 21:1206–1218. https://doi.org/10.1038/s41556-019-0391-5

Magalhaes, J., M.E. Gegg, A. Migdalska-Richards, M.K. Doherty, P.D. Whitfield, and A.H.V. Schapira. 2016. Autophagic lysosome reformation dysfunction in glucocerebrosidase deficient cells: Relevance to Parkinson disease. *Hum. Mol. Genet.* 25:3432–3445. https://doi.org/10.1093/hmg/ddw185

Miyamoto, T., R. DeRose, A. Suarez, T. Ueno, M. Chen, T.P. Sun, M.J. Wolfgang, C. Mukherjee, D.J. Meyers, and T. Inoue. 2012. Rapid and orthogonal logic gating with a gibberellin-induced dimerization system. *Nat. Chem. Biol.* 8:465–470. https://doi.org/10.1038/nchembio.922

Munson, M.J., G.F. Allen, R. Toth, D.G. Campbell, J.M. Lucocq, and I.G. Ganley. 2015. mTOR activates the VPS34-UVRAG complex to regulate autolysosomal tubulation and cell survival. *EMBO J.* 34:2272–2290. https://doi.org/10.15252/embj.201590992

Nagashima, S., L.-C. Tábara, L. Tilokani, V. Paupe, H. Anand, J.H. Pogson, R. Zunino, H.M. McBride, and J. Prudent. 2020. Golgi-derived PI(4)P-containing vesicles drive late steps of mitochondrial division. *Science.* 367:1366–1371. https://doi.org/10.1126/science.aax6089

Nakai, W., Y. Kondo, A. Saitoh, T. Naito, K. Nakayama, and H.-W. Shin. 2013. ARF1 and ARF4 regulate recycling endosomal morphology and retrograde transport from endosomes to the Golgi apparatus. *Mol. Biol. Cell.* 24:2570–2581. https://doi.org/10.1091/mbc.e13-04-0197

Niu, T.-K., A.C. Pfeifer, J. Lippincott-Schwartz, and C.L. Jackson. 2005. Dynamics of GBF1, a Brefeldin A-sensitive Arf1 exchange factor at the Golgi. *Mol. Biol. Cell.* 16:1213–1222. https://doi.org/10.1091/mbc.e04-07-0599

Ostrowski, P.P., G.D. Fairn, S. Grinstein, and D.E. Johnson. 2016. Cresyl violet: A superior fluorescent lysosomal marker. *Traffic.* 17:1313–1321. https://doi.org/10.1111/tra.12447

Parenti, G., D.L. Medina, and A. Ballabio. 2021. The rapidly evolving view of lysosomal storage diseases. *EMBO Mol. Med.* 13:e12836. https://doi.org/10.15252/emmm.202012836

Perera, R.M., and R. Zoncu. 2016. The lysosome as a regulatory hub. *Annu. Rev. Cell Dev. Biol.* 32:223–253. https://doi.org/10.1146/annurev-cellbio-111315-125125

Rong, Y., M. Liu, L. Ma, W. Du, H. Zhang, Y. Tian, Z. Cao, Y. Li, H. Ren, C. Zhang, et al. 2012. Clathrin and phosphatidylinositol-4,5-bisphosphate regulate autophagic lysosome reformation. *Nat. Cell Biol.* 14:924–934. https://doi.org/10.1038/ncb2557

Saffi, G.T., and R.J. Botelho. 2019. Lysosome fission: Planning for an exit. *Trends Cell Biol.* 29:635–646. https://doi.org/10.1016/j.tcb.2019.05.003

Saint-Pol, A., B. Yélamos, M. Amessou, I.G. Mills, M. Dugast, D. Tenza, P. Schu, C. Antony, H.T. McMahon, C. Lamaze, and L. Johannes. 2004.

Clathrin adaptor epsinR is required for retrograde sorting on early endosomal membranes. *Dev. Cell*. 6:525–538. https://doi.org/10.1016/S1534-5807(04)00100-5

Saric, A., S.A. Freeman, C.D. Williamson, M. Jarnik, C.M. Guardia, M.S. Fernandopulle, D.C. Gershlick, and J.S. Bonifacino. 2021. SNX19 restricts endolysosome motility through contacts with the endoplasmic reticulum. *Nat. Commun.* 12:4552. https://doi.org/10.1038/s41467-021-24709-1

Saric, A., V.E.B. Hipolito, J.G. Kay, J. Canton, C.N. Antonescu, and R.J. Botelho. 2016. mTOR controls lysosome tubulation and antigen presentation in macrophages and dendritic cells. *Mol. Biol. Cell*. 27:321–333. https://doi.org/10.1091/mbc.e15-05-0272

Schulze, R.J., S.G. Weller, B. Schroeder, E.W. Krueger, S. Chi, C.A. Casey, and M.A. McNiven. 2013. Lipid droplet breakdown requires dynamin 2 for vesiculation of autolysosomal tubules in hepatocytes. *J. Cell Biol.* 203: 315–326. https://doi.org/10.1083/jcb.201306140

Smith, A.C., J.T. Cirulis, J.E. Casanova, M.A. Scidmore, and J.H. Brumell. 2005. Interaction of the Salmonella-containing vacuole with the endocytic recycling system. *J. Biol. Chem.* 280:24634–24641. https://doi.org/10.1074/jbc.M500358200

Sridhar, S., B. Patel, D. Aphkhazava, F. Macian, L. Santambrogio, D. Shields, and A.M. Cuervo. 2013. The lipid kinase PI4KIIIβ preserves lysosomal identity. *EMBO J.* 32:324–339. https://doi.org/10.1038/emboj.2012.341

Udayar, V., Y. Chen, E. Sidransky, and R. Jagasia. 2022. Lysosomal dysfunction in neurodegeneration: Emerging concepts and methods. *Trends Neurosci.* 45:184–199. https://doi.org/10.1016/j.tins.2021.12.004

Wang, H., H.-Q. Sun, X. Zhu, L. Zhang, J. Albanesi, B. Levine, and H. Yin. 2015. GABARAPs regulate PI4P-dependent autophagosome:lysosome fusion. *Proc. Natl. Acad. Sci. USA*. 112:7015–7020. https://doi.org/10.1073/pnas.1507263112

Wang, Y., Y. Nartiss, B. Steipe, G.A. McQuibban, and P.K. Kim. 2012. ROS-induced mitochondrial depolarization initiates PARK2/PARKIN-dependent mitochondrial degradation by autophagy. *Autophagy*. 8: 1462–1476. https://doi.org/10.4161/auto.21211

Waugh, M.G. 2019. The great escape: How phosphatidylinositol 4-kinases and PI4P promote vesicle exit from the Golgi (and drive cancer). *Biochem. J.* 476:2321–2346. https://doi.org/10.1042/BCJ20180622

Welz, T., J. Wellbourne-Wood, and E. Kerkhoff. 2014. Orchestration of cell surface proteins by Rab11. *Trends Cell Biol.* 24:407–415. https://doi.org/10.1016/j.tcb.2014.02.004

Wenzel, E.M., L.A. Elfmark, H. Stenmark, and C. Raiborg. 2022. ER as master regulator of membrane trafficking and organelle function. *J. Cell Biol.* 221:e202205135. https://doi.org/10.1083/jcb.202205135

Wills, R.C., B.D. Goulden, and G.R.V. Hammond. 2018. Genetically encoded lipid biosensors. *Mol. Biol. Cell*. 29:1526–1532. https://doi.org/10.1091/mbc.E17-12-0738

Wu, H., P. Carvalho, and G.K. Voeltz. 2018. Here, there, and everywhere: The importance of ER membrane contact sites. *Science*. 361:eaan5835. https://doi.org/10.1126/science.aan5835

Yang, C., and X. Wang. 2021. Lysosome biogenesis: Regulation and functions. *J. Cell Biol.* 220:e202102001. https://doi.org/10.1083/jcb.202102001

Yu, L., C.K. McPhee, L. Zheng, G.A. Mardones, Y. Rong, J. Peng, N. Mi, Y. Zhao, Z. Liu, F. Wan, et al. 2010. Termination of autophagy and reformation of lysosomes regulated by mTOR. *Nature*. 465:942–946. https://doi.org/10.1038/nature09076

Zhu, Y., S. Li, A. Jaume, R.A. Jani, C. Delevoye, G. Raposo, and M.S. Marks. 2022. Type II phosphatidylinositol 4-kinases function sequentially in cargo delivery from early endosomes to melanosomes. *J. Cell Biol.* 221: e202110114. https://doi.org/10.1083/jcb.202110114
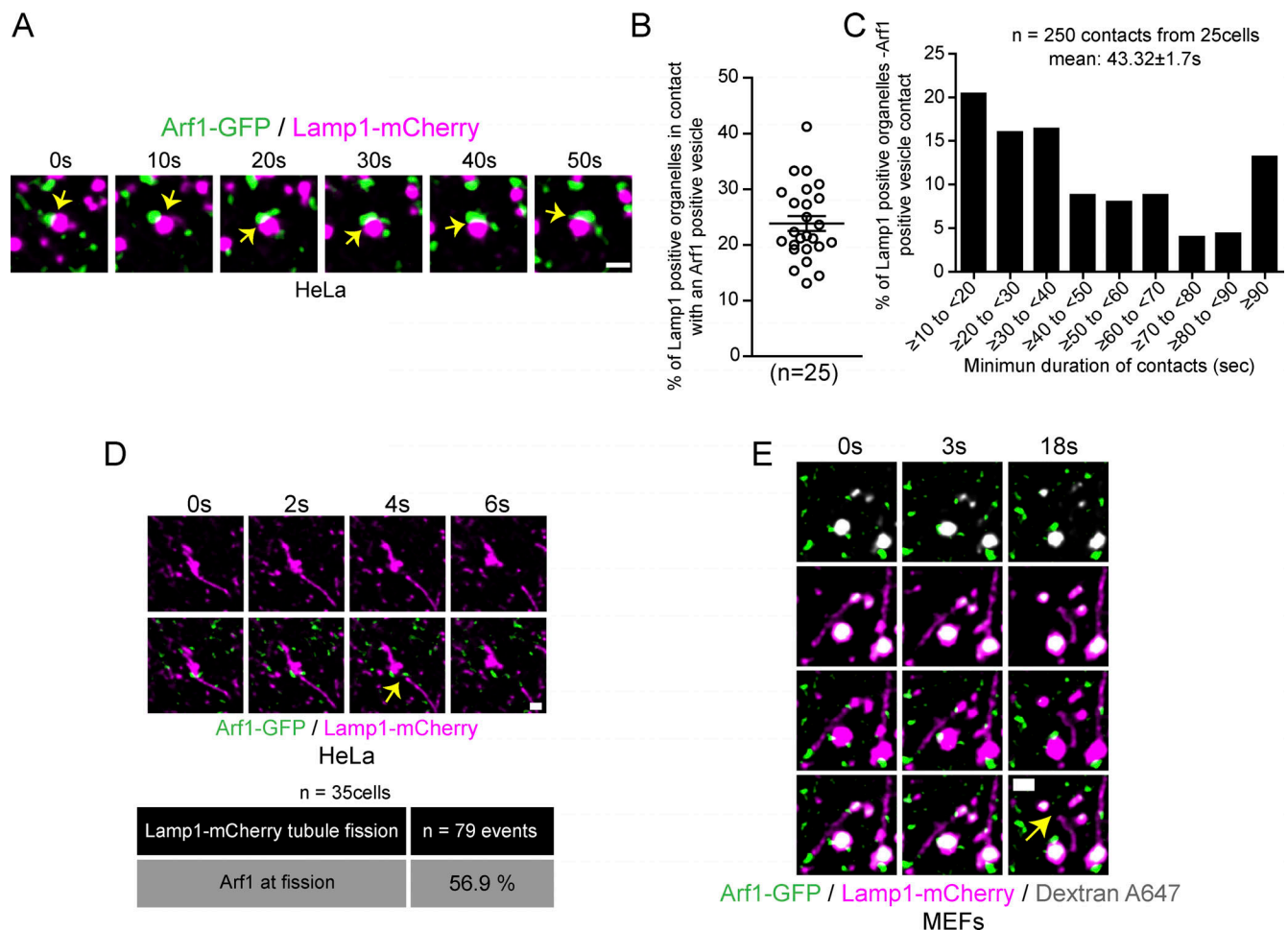
Figure S1. **Arf1 positive vesicles make stable and dynamic contacts with Lamp1 positive organelles in HeLa cells and mark lysosomal tubule fission sites. (A)** Representative time-lapse live images showing dynamic contact between Arf1-GFP positive vesicles and Lamp1 positive organelles in HeLa cells. Yellow arrow points to contacts between these two compartments. Scale bar: 1 μm. **(B)** Quantification of the percentage of Lamp1 positive organelles in contact with at least one Arf1 positive vesicle in HeLa cells. The graphs show the mean ± SEM, cells from three independent experiments. **(C)** Quantification of the mean minimum duration (seconds) of Lamp1 positive organelle-Arf1 positive vesicle contacts. A contact is defined by overlapping pixels, and the time of contact was quantified from time-lapse images taken at one frame every 2 s. 250 randomly chosen contacts from 25 cells were analyzed. **(D)** Representative time-lapse imaging showing an Arf1-GFP positive vesicle marking the fission site of tubule from a Lamp1-mCherry positive organelle in a HeLa cell starved for 8 h with HBSS (amino acid-free media) in order to promote formation and fission of Lamp1 tubules. Yellow arrow indicates the fission event. Scale bar: 1 μm. The percentage of tubule fission events marked by Arf1-GFP vesicles was quantified. *n* = 79 events from 35 HeLa cells. **(E)** Representative time-lapse imaging showing an Arf1-GFP vesicle marking fission site of a tubule from a lysosome in a MEF cell. Lysosomes were identified as organelles positive for Lamp1 and overnight chased fluorescent 10 kD Dextran. Yellow arrow indicates fission. Scale bar: 1 μm.

A

n=19 cells

Lamp1 tubules fission	n = 38 events
ER at fission	92.1 %
Arf1 at fission	63.1 %
ER and Arf1 at fission	57.9 %

Arf1-BFP / GFP-KDEL / Lamp1-mCherry
COS7

B

ub-GFP-SKL / Lamp1-mCherry
MEFs

n = 22 cell

Lamp1 tubule division	n = 49 events
ub-GFP-SKL positive	20.4 %
90° rotated control	20.5 %

C

GFP-PI4KIIIβ / Lamp1-mCherry / Dextran 647
MEFs

D

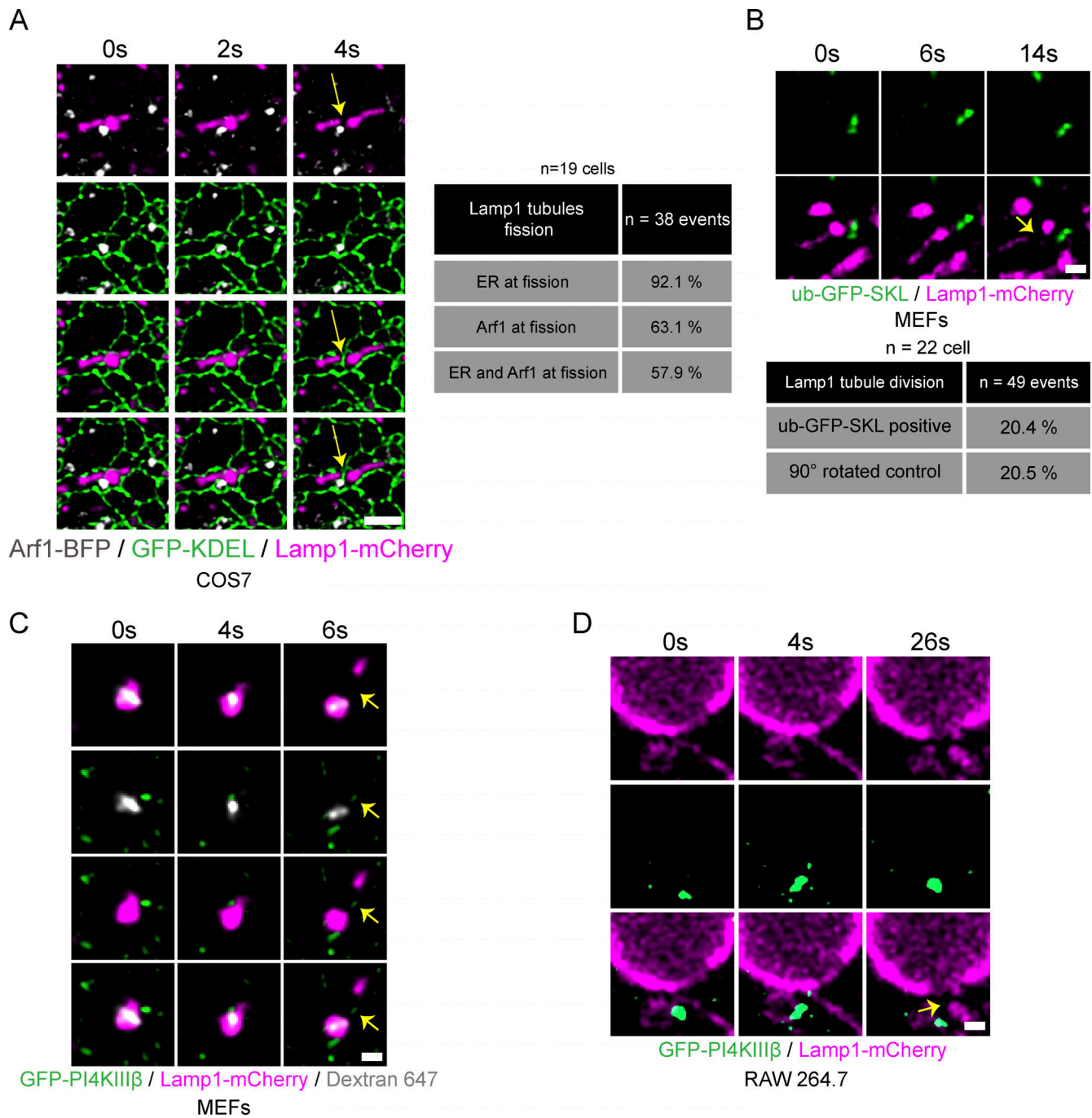GFP-PI4KIIIβ / Lamp1-mCherry
RAW 264.7

Figure S2.   **The ER is present at Lamp1 tubule fission sites marked by Arf1 positive vesicles and PI4KIIIβ positive vesicles are found at endolysosomal and phagolysosomal tubule fission sites. (A)** Time-lapse imaging of a COS7 cell expressing the ER marker GFP-KDEL, Arf1-BFP, and Lamp1-mCherry incubated for 8 h in HBSS media that shows the concomitant presence of the ER and of an Arf1 positive vesicle to a Lamp1 positive tubule fission event. Quantification of such event is shown in the table. n = 38 events from 19 cells. Yellow arrow indicates fission. Scale bar: 2 μm. **(B)** Representative time-lapse images showing the absence of ub-GFP-SKL (Peroxisome) at a Lamp1 positive tubule fission site in MEFs starved (HBSS) for 8 h and quantification of percentage of fission events marked by ub-GFP-SKL. Negative control analysis was performed with the Lamp1-mCherry signal rotated by 90°. n = 49 events from 22 cells. Yellow arrows indicate fission. Scale bar: 1 μm. **(C and D)** Representative time-lapse imaging showing a GFP-PI4KIIIβ positive vesicle marking fission site of a tubule from an **(C)** endolysosome in a MEF cell. Endolysosomes were formed by 24 h incubation with sucrose and their tubulation and fission was observed after 1 h of treatment with invertase (0.5 mg/ml). Endolysosomes were defined as positive for Lamp1 and overnight chased fluorescent 10 kD Dextran; **(D)** Phagolysosome in RAW264.7 cells phagocytosing SRBCs. Yellow arrows indicate fission. Scale bar: 1 μm.
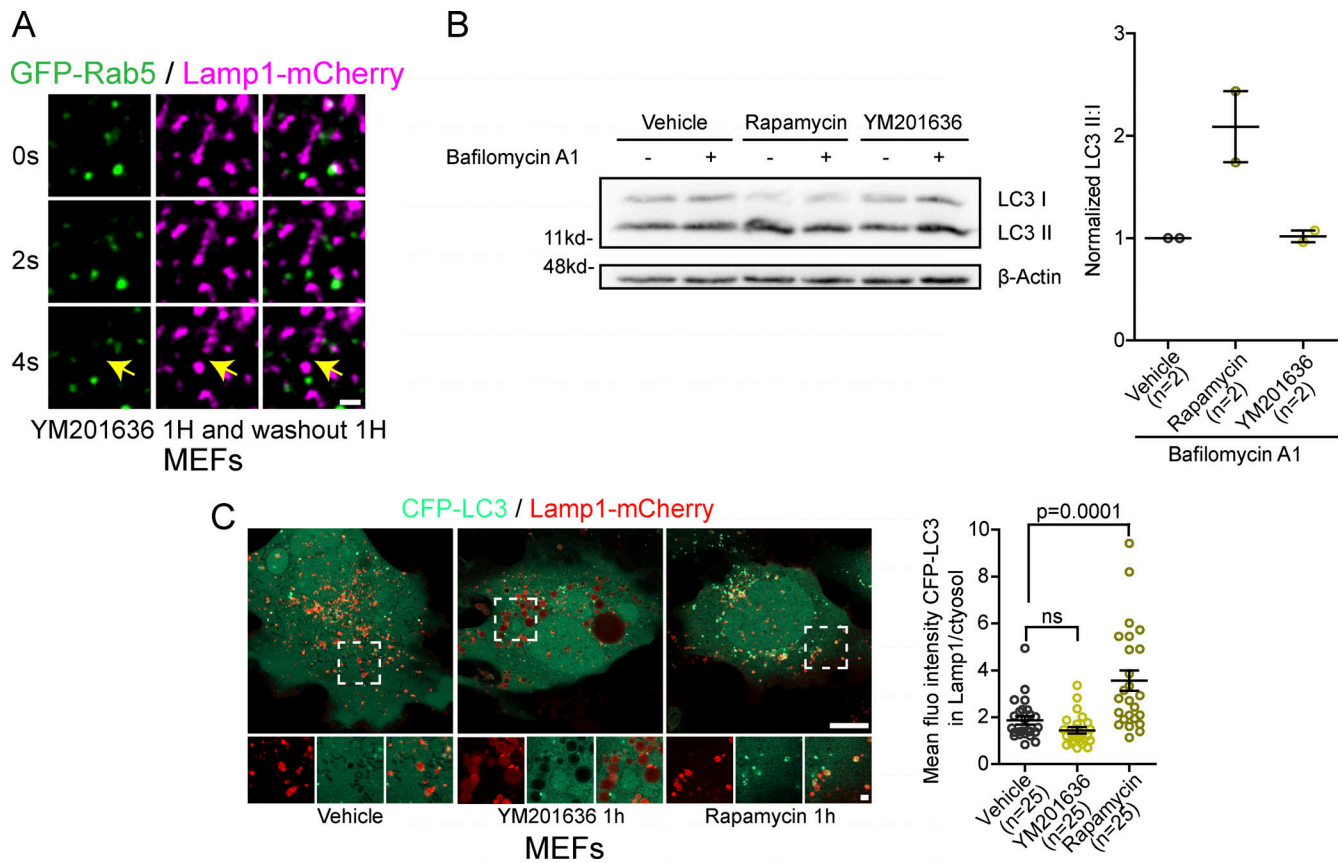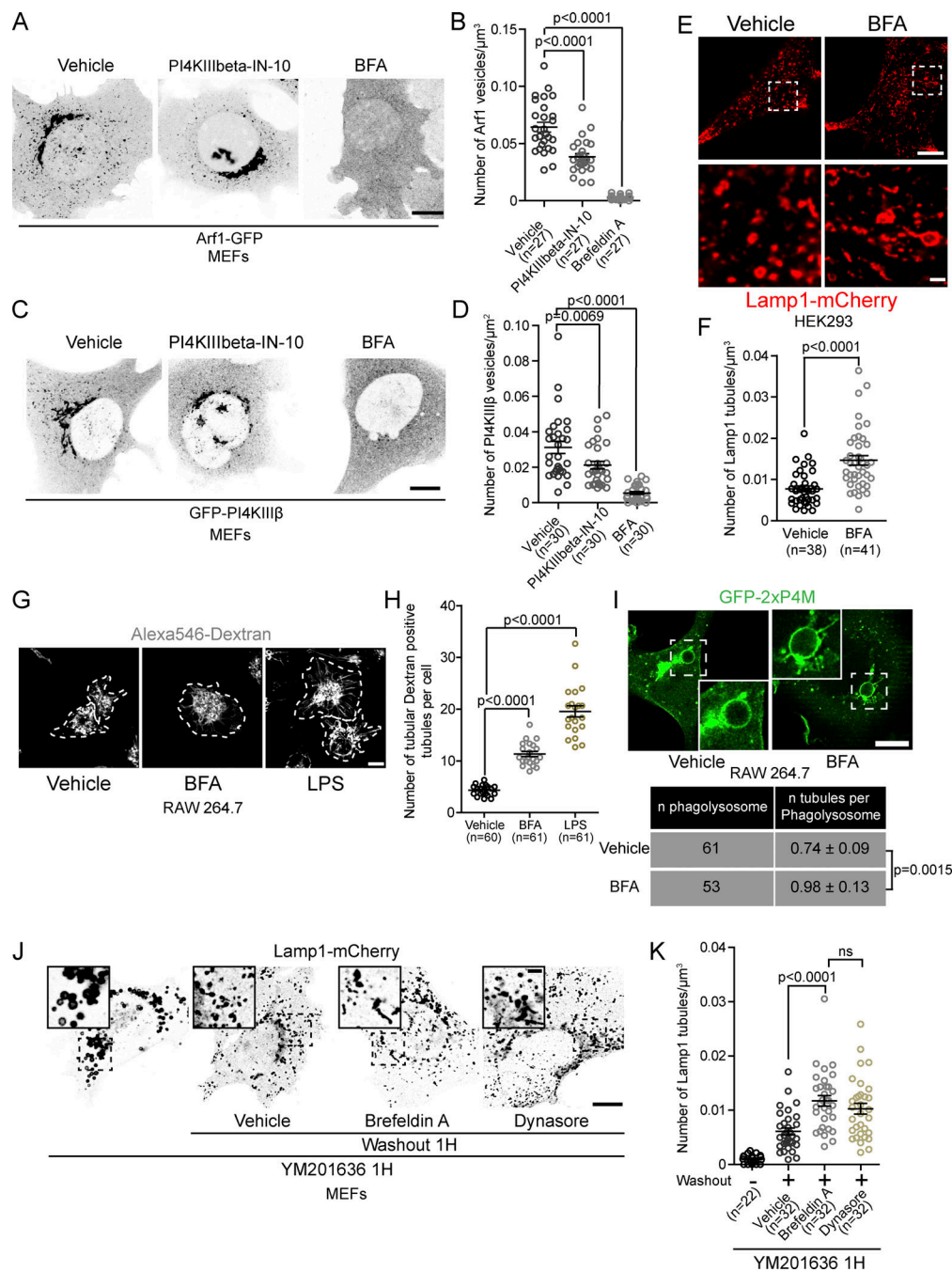
Figure S3. **Short-term inhibition of PIKfyve with YM201636 does not induce autophagy or formation of endolysosomes. (A)** Time-lapse imaging of a Lamp1 positive tubule fission event in a MEF cell expressing Rab5-GFP and Lamp1-mCherry after short-term inhibition of PIKfyve using YM2013636 (1 μM for 1 h) followed by 1 h washout of the drug. The yellow arrows indicate tubule fission. Scale bar = 1 μm. **(B)** Representative Western blot images of MEFs treated 1 h with YM201636 (1 μM) or vehicle control, rapamycin (10 μg/ml) was used as a positive control. Bafilomycin A1 treatment (500 nM, 1 h) was used to inhibit degradation of autophagosomes allowing to evaluate whether YM201636 treatment induced formation of autophagosomes. Levels of LC3 II were normalized to LC3 I to quantify autophagosomes. β-Actin was used as a loading control. The graphs show the mean ± SEM, cells from two independent experiments. **(C)** Representative images of MEFs cells expression CFP-LC3 and Lamp1-mCherry and treated with YM201636 (1 μM for 1 h) or Rapamycin (10 μg/ml) as a positive control. Scale bars: 10 and 2 μm (inset). Quantification of the mean fluorescence intensity of CFP-LC3 colocalizing with Lamp1 normalized to that of the cytosol. The graphs show the mean ± SEM, cells from three independent experiments. One-way ANOVA with Dunnett's multiple comparison test. ns = 0.4570. Source data are available for this figure: SourceData FS3.

Boutry et al.
Lysosome tubules fission by Arf1-PI4KIIIβ vesicles

Journal of Cell Biology   S3
https://doi.org/10.1083/jcb.202205128

Figure S4. **Inhibition of formation and/or function of Arf1-PI4KIIIβ positive vesicles increases the number of lysosomal tubules. (A)** Representative images of MEFs expressing Arf1-GFP and treated with PI4KIIIbeta-IN-10 (25 nM, 3 h) or BFA (10 µg/ml, 1 h). Ethanol was used as a vehicle control. Scale bar: 10 µm. **(B)** Quantification of the number of Arf1-GFP positive vesicles per cell. One-way ANOVA with Dunnett's multiple comparison test. **(C)** Representative images of MEFs expressing GFP-PI4KIIIβ and treated with PI4KIIIbeta-IN-10 (25 nM, 3 h) or BFA (10 µg/ml, 1 h). Ethanol was used as a vehicle control. Scale bar: 10 µm. **(D)** Quantification of the number of GFP-PI4KIIIβ positive vesicles per cell. One-way ANOVA with Dunnett's multiple comparison test. **(E)** Representative images of HEK293 cells expressing Lamp1-mCherry and treated with BFA (10 µg/ml, 1 h) or ethanol as a vehicle control. Scale bars: 10 and 1 µm (inset; F) Quantification of the number of Lamp1 positive tubules in these cells. Two-sided unpaired *t* test. **(G)** Representative images of primary mouse macrophages that were pulsed with Alexa546-Dextran (50 µg/ml, 30 min) to mark lysosomes and treated with BFA (5 µg/ml, 2 h). LPS (500 ng/ml, 2 h) was used as a positive control. DMSO was used as a negative control (vehicle). Images were acquired using a Spinning disk confocal microscope system (Quorum Technologies). White dotted lines show cell outline. Scale bar: 10 µm. **(H)** Quantification of the number of Dextran positive tubules in these cells. One-way ANOVA with Dunnett's multiple comparison test. **(I)** Representative images of phagolysosomes from RAW264.7 macrophages expressing GFP-2xP4M and treated with BFA (10 µg/ml) 15 min after induction of phagocytosis of SRBCs. Cells were imaged from 15 to 30 min after BFA was added. Ethanol was used as vehicle. Scale bar: 10 µm. Quantification of the number of tubules from these cells. Two-sided unpaired *t* test. **(J)** Representative images of MEFs expressing Lamp1-mCherry. Cells were treated with YM201636 (1 µM, 1 h) to inhibit PIKfyve and were then washed out to remove PIKfyve inhibitor in presence of BFA (10 µg/ml) or Dynasore (40 µM) and imaged 1 h after. Scale bars: 10 and 2 µm (inset). **(K)** Quantification of the number of Lamp1 positive tubules from these cells. One-way ANOVA with Dunnett's multiple comparison test. All graphs (B, D, F, H and K) show the mean ± SEM, cells from three independent experiments.
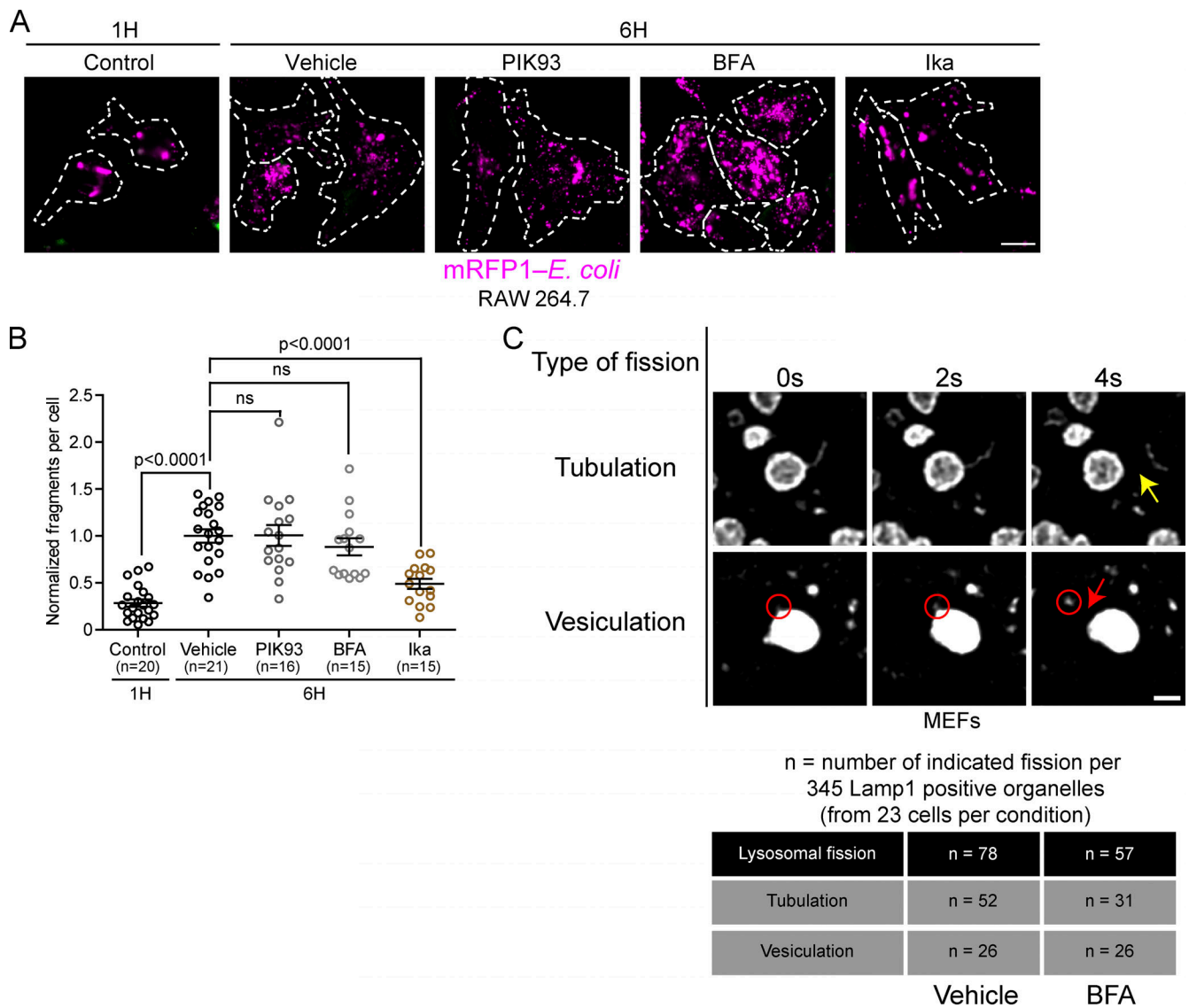
Figure S5. Inhibition of PI4KIIIβ or Arf1 activation does not affect lysosomal fission by vesiculation and splitting. (A) Representative images of phagosome fragmentation in RAW 264.7 that were allowed to internalize mRFP1-labeled *E. coli* (magenta), then washed and incubated for 1 or 6 h before imaging. Cells were treated with either DMSO, 10 µM PIK93, 10 µM BFA, or 0.5 µg/ml Ikarugamycin (Ika) 1 h after phagocytosis and imaged at indicated times. Cells were labeled with anti-*E. coli* (green) to identify external bacteria. Images were acquired using a Spinning disk confocal microscope system (Quorum Technologies). Scale bar = 10 µm. **(B)** Quantification of the number of mRFP-*E. coli* positive fragments in these cells. The graphs show the mean ± SEM, cells from three independent experiments. Statistical analysis was performed using the Kruskal–Wallis test with Dunn's multiple comparisons test. ns: P > 0.9999 (Vehicle vs. PIK93) and P = 0.8132 (Vehicle vs. BFA). **(C)** MEF cells expressing Lamp1-mCherry were treated with the PIKfyve inhibitor YM201636 (1 µM for 1 h) and then PIKfyve inhibitor was washed out in presence of BFA (10 µg/ml) or a vehicle control (ethanol). Cells were imaged between 5 and 30 min after washout. A total of 345 Lamp1 positive organelles (from 23 cells) per condition were analyzed for two types of lysosomal fission: fission of tubules (tubulation) or of vesicles (vesiculation). The yellow arrow indicates tubule fission while the red circle indicates a vesiculation event and the red arrow the fission of this vesicle from the lysosome. Scale bar: 1 µm.

Boutry et al.
Lysosome tubules fission by Arf1-PI4KIIIβ vesicles

Journal of Cell Biology S5
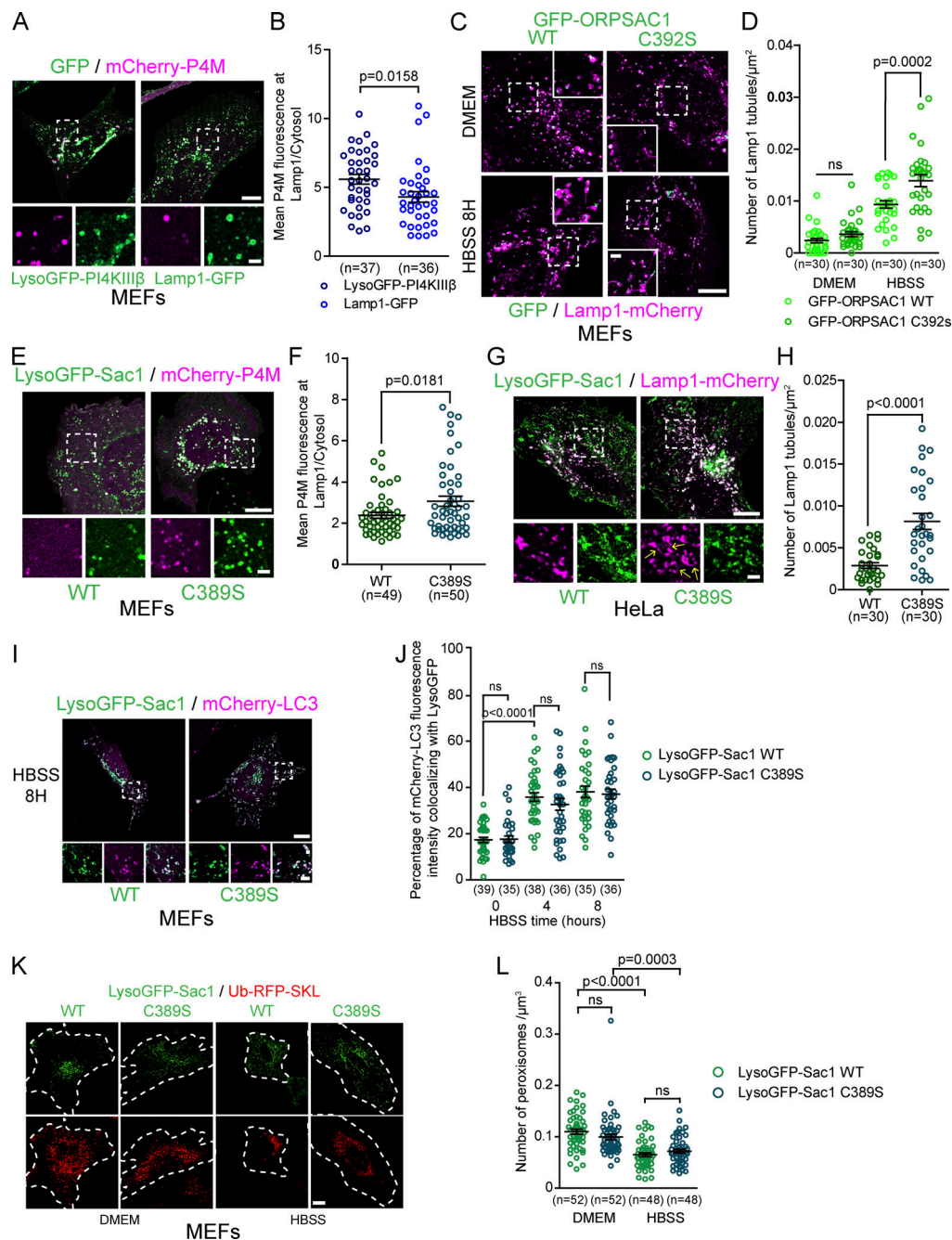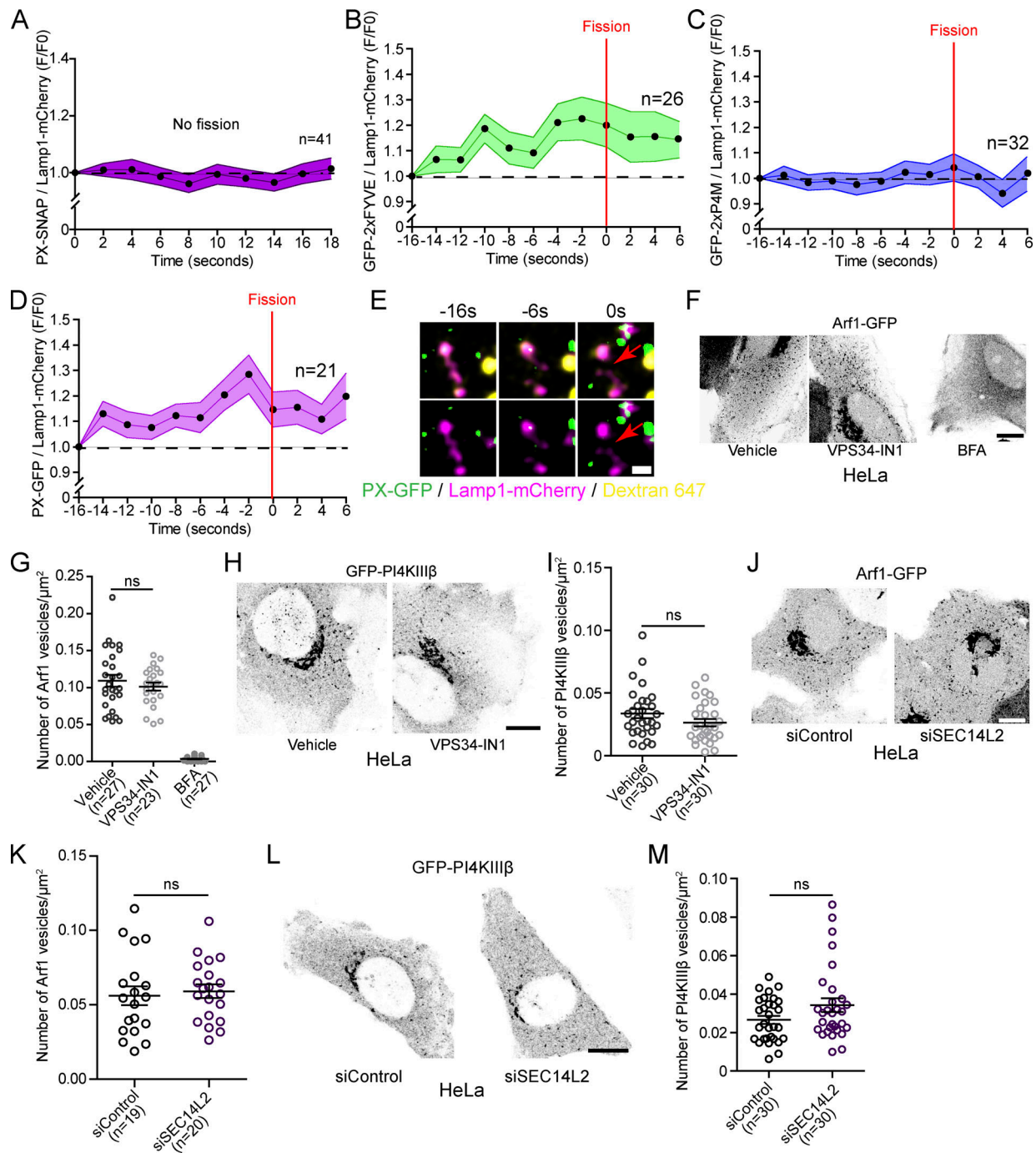https://doi.org/10.1083/jcb.202205128

Figure S6. **Depletion of lysosomal PI(4)P impairs formation of Lamp1 positive tubules but does not affect the fusion of lysosomes with autophagosomes. (A)** Representative images of MEFs expressing mCherry-P4M and LysoGFP-PI4KIIIβ or Lamp1-GFP. Scale bars: 10 and 2 μm (inset). **(B)** Quantification of the P4M fluorescence intensity in Lamp1 mask normalized by the cytosolic one. Two-sided unpaired t test. **(C)** Representative images of MEF cells expressing Lamp1-mCherry or GFP-ORPSAC1 to deplete lysosomal PI(4)P. The catalytic dead version of ORPSAC1 (C392S) was used as a negative control. Cells were treated with HBSS for 8 h to promote formation of tubules from Lamp1 positive organelles. Scale bars: 10 and 2 μm (inset). **(D)** Quantification of the number of Lamp1 positive tubules for these cells. Two-way ANOVA with Tukey's multiple comparisons test. ns: 0.6594. **(E)** Representative images of MEFs expressing mCherry-P4M and LysoGFP-Sac1 or the catalytic dead version of it (C389S). Scale bars: 10 and 2 μm (inset). **(F)** Quantification of the P4M fluorescence intensity in Lamp1 mask normalized by the cytosolic one. Two-sided unpaired t test. **(G)** Representative HeLa cells expressing Lamp1-mCherry and LysoGFP-Sac1 or the catalytic dead version of it (C389S). Cells were treated with HBSS to promote formation of tubules from autolysosomes. Yellow arrow in the inset point to Lamp1 tubules. Scale bars: 10 and 2 μm (inset). **(H)** Quantification of the number of tubules from these cells. Two-sided unpaired t test. **(I)** Representative images of MEF cells expressing mCherry-LC3 and LysoGFP-Sac1 or the catalytic dead version of it (C389S). Cells were treated with HBSS to promote formation of autophagosomes and their fusion with lysosomes. Scale bars: 10 and 2 μm (inset). **(J)** Quantification of the percentage of mCherry-LC3 staining colocalizing with LysoGFP at indicated time of HBSS treatment. Two-way ANOVA with Tukey's multiple comparisons test. ns: P > 0.9999 (0 h), P = 0.9456 (4 h) and P > 0.9999 (8 h). **(K)** Representative images of MEF cells expressing the peroxisomal marker ub-RFP-SKL and LysoGFP-Sac1 or the catalytic dead version of it (C389S). Cells were treated with HBSS for 24 h to promote removal of peroxisomes by the autophagic pathway. Scale bar: 10 μm. **(l)** Quantification of the number of peroxisomes per area for these cells. Two-way ANOVA with Tukey's multiple comparisons test. ns: P = 0.3683 and P = 0.7442. (B, D, F, H, J, and L). All graphs show the mean ± SEM, cells from three independent experiments.

Boutry et al.
Lysosome tubules fission by Arf1-PI4KIIIβ vesicles

Journal of Cell Biology S6
https://doi.org/10.1083/jcb.202205128

Figure S7. **PI(3)P and PI(4)P levels during Lamp1 positive tubule fission events and SEC14L2 depletion or VPS34-IN1 do not affect Arf1-PI4KIIIβ positive vesicles formation. (A)** Normalized fluorescence intensity of PX (PI(3)P biosensor) at Lamp1 positive organelles with tubules that are not undergoing any fission events. MEFs were starved (HBSS) for 8 h to promote formation of tubules from Lamp1 positive organelles. **(B)** Normalized fluorescence intensity of 2xFYVE (PI(3)P biosensor) at Lamp1 positive organelles during tubule fission events. MEFs were starved (HBSS) for 8 h. **(C)** Normalized fluorescence intensity of 2xP4M (PI(4)P biosensor) at Lamp1 positive organelles during tubule fission events. MEFs cells were starved (HBSS) for 8 h. **(D)** Normalized fluorescence intensity of PX (PI(3)P biosensor) at lysosomes (Lamp1 and overnight chased fluorescent 10 kD Dextran). MEFs were starved (HBSS) for 8 h. Red arrows indicate fission. Scale bar: 1 μm. **(E)** Representative time-lapse image of a Lamp1 fission event from a Lamp1 and overnight chase Dextran 647 positive organelle analyzed in MEFs expressing the PI(3)P biosensor PX-GFP. Red arrows indicate fission. Scale bar: 1 μm. **(F)** Representative images of HeLa cells expressing Arf1-GFP and treated with VPS34-IN1 (1 μM) or BFA (10 μg/10 ml) for 1 h. Scale bar: 10 μm. **(G)** Quantification of the number of Arf1-GFP positive vesicles per cell. One-way ANOVA with Dunnett's multiple comparison test. ns = 0.5088. **(H)** Representative images of HeLa cells expressing GFP-PI4KIIIβ and treated with the indicated drug for 1 h. Ethanol was used as a vehicle control. Scale bar: 10 μm. **(I)** Quantification of the number of GFP-PI4KIIIβ positive vesicles in these cells. Two-sided unpaired *t* test. ns = 0.1194. **(J)** Representative Airyscan images of HeLa cells expressing Arf1-GFP and treated with indicated siRNAs. Scale bar: 10 μm. **(K)** Quantification of the number of Arf1-GFP positive vesicles per cell. Two-sided unpaired *t* test. ns = 0.6999. **(L)** Representative images of HeLa cells expressing GFP-PI4KIIIβ and treated with the indicated siRNAs. **(M)** Quantification of the number of GFP-PI4KIIIβ positive vesicles in these cells. Two-sided unpaired *t* test. ns = 0.0676. (A–D, G, I, K, and M). All graphs show the mean ± SEM, cells from two independent experiments.

Video 1.   **Arf1 positive vesicles and Lamp1 positive organelles appear to form dynamic contacts.** Movie relative to Fig. 1 C: Representative time-lapse fluorescent microscopy images of a Lamp1 positive organelle-Arf1 positive vesicle contact. MEF cell expressing Arf1-GFP (green) and Lamp1-mCherry (magenta). Five frames per second. Frame interval is 2 s.

Video 2.   **Arf1 positive vesicles are recruited to Lamp1 positive tubule fission sites.** Movie relative to Fig. 1 F: Three-dimensional reconstruction of time-lapse fluorescent microscopy images, acquired with a lattice light sheet microscope, of a Lamp1 positive tubule fission event showing recruitment of a Arf1 positive vesicle at the site of fission. MEF cell expressing Arf1-GFP (green) and Lamp1-mCherry (magenta). One frame per second. Frame times are indicated in Fig. 1 F.

Video 3.   **Arf1 positive vesicles are recruited to sites of autolysosomal tubule fission.** Movie relative to Fig. 3 B: Representative time-lapse fluorescent microscopy images of an autolysosomal tubule fission event showing recruitment of an Arf1 positive vesicle at the site of fission. COS7 cell expressing Arf1-GFP (green), Lamp1-SNAP(647) (magenta) and mCherry-LC3 (gray) and incubated in amino acid free media (HBSS) for 8 h. Five frames per second. Frame interval is 2 s.

Video 4.   **Arf1 positive vesicles are recruited to sites of phagolysosomal tubule fission.** Movie relative to Fig. 3 F: Representative time-lapse fluorescent microscopy images of phagolysosomal tubule fission event showing recruitment of an Arf1 positive vesicle at the site of fission. RAW 264.7 cells expressing Arf1-GFP (green) and Lamp1-mCherry (magenta) undergoing phagocytosis of opsonized SRBCs (Sheep Red Blood Cells). Phagocytosis was synchronized by centrifugation (10 s at 300 G). One frame per second. Frame interval is 3 s.

Provided online is Table S1. Table S1 lists primers used for cloning (see Plasmids section in Materials and methods).